https://doi.org/10.5194/bg-2020-156
Preprint. Discussion started: 25 May 2020

Biogeosciences Discussions

Variable phytoplankton size distributions reduce the sensitivity of global export flux to climate change

Shirley W. Leung[1], Thomas Weber[1,2], Jacob A. Cram[1,3], Curtis Deutsch[1]

[1]School of Oceanography, University of Washington, Seattle, 98195, US
[2]Department of Earth and Environmental Science, University of Rochester, Rochester, 14627, US
[3]Horn Point Laboratory, University of Maryland Center for Environmental Science, Cambridge, 21613, US

Correspondence to: Shirley W. Leung (shirlleu@uw.edu)

Abstract. Earth System Models predict a 10-20% decrease in ocean carbon export production by the end of the 21st century due to global climate change. This decline is caused by increased stratification of the upper ocean, resulting in reduced shallow subsurface nutrient concentrations and a slower supply of nutrients to the surface euphotic zone. These predictions, however, do not account for associated changes in sinking particle size and remineralization depth. Here we combine satellite-derived export and particle size maps with a simple 3-D global biogeochemical model to investigate how shifts in sinking particle size may buffer predicted changes in surface nutrient supply and therefore export production. We show that higher export rates are correlated with larger phytoplankton and sinking particles, especially in tropical and subtropical regions. Incorporation of these empirical relationships into a global model shows that as circulation slows, a decrease in export and associated shift toward smaller phytoplankton yields particles that sink more slowly and are thus remineralized shallower; this in turn leads to greater recycling of nutrients in the upper water column and faster nutrient recirculation into the euphotic zone, boosting productivity and export to counteract the initial circulation-driven decreases. This negative feedback mechanism (termed the particle size-remineralization feedback) slows export decline over the next century by ~14% globally and by ~20% in the tropical and subtropical oceans, where export decreases are currently predicted to be greatest. Thus, incorporating dynamic particle size-dependent remineralization depths into Earth System Models will result in more robust predictions of changes in biological pump strength in a warming climate.

1 Introduction

1.1 Carbon export in the future ocean

A key mechanism that controls the partitioning of carbon dioxide (CO_2) between the atmosphere and ocean is the biological pump, in which CO_2 is fixed into phytoplankton organic matter via photosynthesis, and then exported from the surface to the deep ocean as sinking particles (e.g., Ducklow et al., 2001). Decomposition of this particulate organic carbon (POC) in the ocean interior maintains a reservoir of respired CO_2 that is sequestered out of contact with the atmosphere, thus exerting an important control on long-term atmospheric CO_2 concentrations and global

https://doi.org/10.5194/bg-2020-156
Preprint. Discussion started: 25 May 2020


Biogeosciences Discussions Open Access EGU

climate (e.g., Martínez-García et al., 2014; Passow & Carlson, 2012; Sarmiento & Siegenthaler, 1992). Carbon exported out of the surface euphotic zone also fuels the metabolism of organisms in the mesopelagic zone, sustaining economically and socially important fisheries, as well as ecologically important zooplankton and micronekton communities (e.g., Boyd et al., 2019; Friedland et al., 2012). POC export is also an important driver of dissolved oxygen concentrations in the water column. Where sinking POC fluxes are particularly high, enhanced bacterial breakdown of particles can deplete available oxygen and create hypoxic or even suboxic conditions in which many organisms cannot survive (e.g., Hofmann and Schellnhuber, 2009; Oschlies et al., 2008). Given the critical role of POC export in driving ocean carbon sequestration, the global climate system, fisheries productivity, and dissolved oxygen availability, there is a growing need to better understand how export will respond to future climate warming.

State-of-the-art Earth System Models (ESMs) predict decreases in global export production (defined as the sinking POC flux at 100m) of ~10-20% by 2100 (Bopp et al., 2013; Cabré et al., 2015a) and ~30% by 2300 (Moore et al., 2018). In these models, primary production and subsequent carbon export are largely limited by the physical supply of nutrients to the surface ocean, which is predicted to slow with future warming. Mechanisms driving this nutrient supply slowdown include: (i) surface warming-induced stratification of the water column, which will shoal winter mixed layers, limit vertical exchange, and "trap" nutrients in the ocean interior (Bopp et al., 2013; Cabré et al., 2015a; Capotondi et al., 2012; Moore et al., 2018), and (ii) a weakening of the trade winds, which will reduce upwelling rates and vertical nutrient supply in tropical oceans (Bopp et al., 2001; Collins et al., 2010), as well as lateral Ekman-driven nutrient supply into the subtropics (Letscher et al., 2016).

Changes in the POC flux itself, however, also have the potential to modulate nutrient supply to the surface ocean and therefore impact export. Because particles release nutrients when they decompose, the depth scale of particle remineralization determines the proximity of these nutrients to the surface and their resupply rate to the euphotic zone (Kwon et al., 2009; Yamanaka & Tajika, 1996). Shallow remineralization in mesopelagic waters, especially above the permanent pycnocline, drives rapid nutrient recirculation to the surface; nutrients remineralized in deeper waters, on the other hand, can take hundreds of years to re-emerge at the surface (Martin et al., 1987; Matsumoto, 2007). This raises the possibility of feedback loops in which changes in particle remineralization depth might either dampen or enhance circulation-driven decreases in primary production and export.

Recent work has shown that particle size plays a paramount role in determining remineralization length scales and carbon transfer efficiency to depth due to its influence on sinking speed (Cram et al., 2018; Kriest & Oschlies, 2008; Weber et al., 2016). Current ESMs, however, generally do not resolve a dynamic particle size spectrum and so cannot fully capture biological feedbacks driven by particle size (Laufkötter et al., 2016; Le Quéré et al., 2005). For example, it is common in global models to impose a power-law particle flux profile based on empirical fits to sediment trap measurements (Bopp et al., 2001; Kwon et al., 2009; Maier-Reimer, 1993; Martin et al., 1987; Najjar et al., 1992; Yamanaka & Tajika, 1996), or to explicitly simulate particles whose sinking speeds are fixed, vary over depth (Aumont & Bopp, 2006; Schmittner et al., 2005), or differ between only one large and one small size class (Aumont & Bopp, 2006; Gregg et al., 2003). More complex models that resolve aggregation-disaggregation transformations and/or continuous particle sizes have been developed (Gehlen et al., 2006; Kriest & Oschlies, 2008), but have not

https://doi.org/10.5194/bg-2020-156
Preprint. Discussion started: 25 May 2020

been used to study the effects of climate change on export production. Furthermore, parameters and processes in most previous models are not constrained by observations of particle size distributions.

Here we conduct a series of model experiments constrained by empirical relationships to isolate the effect of particle size-dependent remineralization depths on future export changes. We use satellite-derived export rates and particle size data in combination with a 3-D global biogeochemical model to demonstrate that current ESMs, which lack particle size-dependent remineralization depths, may overestimate 21st century decreases in carbon export.

1.2 A hypothesized particle size-remineralization (PSR) feedback

Particle abundances in the ocean tend to follow a power-law distribution with many more small particles than large ones (Boss et al., 2001; Sheldon et al., 1972). Particle size distributions can thus be succinctly described by the negative exponent in the power-law relationship between particle diameter and number density, i.e. the negative linear slope between these two variables on log-log axes. We define the absolute value of this slope as β. A shallower slope (small β) indicates a greater proportion of large particles relative to small ones, while a steeper slope (large β) indicates a smaller proportion of large particles.

Large particles tend to exist in the ocean where larger microphytoplankton (>20 um in diameter) are dominant, while relatively small particles tend to exist where smaller picophytoplankton (<2 um in diameter) are dominant (Guidi et al., 2007; Guidi et al., 2008; Guidi et al., 2009). The presence of large phytoplankton leads to the generation of larger particles perhaps because large phytoplankton are more likely to form aggregates and be transformed into large fecal pellets by large zooplankton, whereas small phytoplankton are more likely to be degraded by bacteria and consumed by smaller zooplankton (Bopp et al., 2005; Guidi et al., 2007; Guidi et al., 2009; Michaels and Silver, 1988). The exact mechanisms governing the processes by which smaller and larger phytoplankton become smaller and larger particles are not clearly known, however, and is an active area of research.

Phytoplankton community size structure is in turn determined by the availability of nutrients. Low-nutrient conditions select for small phytoplankton with high surface area-to-volume ratios, which make them less susceptible to nutrient diffusion limitation (Litchman et al., 2007). Regions with lower nutrient concentrations thus tend to have a greater relative abundance of small picophytoplankton and particles, while regions with higher nutrient concentrations tend to be dominated by larger microphytoplankton and particles. Indeed, global patterns of annual-mean β (Kostadinov et al., 2009) and fractional picophytoplankton abundance (fpico) (Hirata et al., 2011) estimated from remote sensing correspond closely with surface nutrient concentrations (Fig. 1a-c).

Past work has also firmly established a strong positive relationship between particle size and sinking speed in the ocean (Alldredge and Gotschalk, 1988; Smayda, 1971) (although there are exceptions to this rule, particularly in the Southern Ocean – see McDonnell and Buesseler (2010)). The characteristic depth scale of particle remineralization is proportional to this sinking speed divided by a microbially-mediated remineralization rate (Kwon et al., 2009; McDonnell et al., 2015). Here we define remineralization depth as the shallowest depth at which POC flux out of the euphotic zone is reduced by a factor of e or 63% (i.e., the e-folding depth of the flux) (Fig. 1d). The dominance of smaller phytoplankton and sinking particles in the water column results in a shallower remineralization

https://doi.org/10.5194/bg-2020-156
Preprint. Discussion started: 25 May 2020

depth, as bacteria have more time to remineralize these slow-sinking particles in the upper layers of the water column (Bach et al., 2016).

In sum, there are strong connections between nutrient availability, phytoplankton community structure, particle size, and remineralization depth, as evidenced by their closely-related global patterns (Fig. 1). Taken together, these connections point towards a negative feedback loop that may dampen changes in carbon export arising from physically-induced changes in surface nutrient supply. In a warming and stratifying ocean, this hypothesized feedback (hereafter known as the particle size-remineralization feedback, or PSR feedback) would proceed through the following steps, which are illustrated schematically in Fig. 2:

1.) Slower Circulation (SC) – First, stratification of the water column and slowing trade winds with climate warming will reduce shallow subsurface nutrient concentrations and vertical exchange/upwelling rates. This slows nutrient supply into the euphotic zone, which in turn decreases phytoplankton productivity and resultant export production (Fig. 2a, b, green arrows).

2.) Ecological Effect (EE) – A decrease in surface nutrient supply also selects for smaller phytoplankton, which leads to a larger proportion of small particles in the export flux. The net result of this ecological effect (EE) (Fig. 2a, red arrow) can be captured by the relationship between export and β (Fig. 2c, red line), as any decrease in export driven by decreased nutrient supply would also cause a corresponding decrease in phytoplankton/particle size. The degree to which particle sizes shrink in association with decreasing export rates is represented by the negative slope of the red, theoretical export-versus-β line in Fig. 2c. Constrained by this relationship, the changes in export and β under slowed circulation (SC) must fall along this red line ("SC with EE" point). In the absence of the ecological effect (i.e., phytoplankton/particle sizes are not affected by changes in the nutrient supply), there is no such requirement and β would remain unchanged under a slowed circulation scenario ("SC without EE" point in Fig. 2c).

3.) Sinking Speed Effect (SSE) – Smaller particles resulting from the ecological response to a reduced nutrient supply would sink more slowly and therefore remineralize shallower in the water column. More regenerated nutrients would then accumulate within shallower waters and thus recirculate more quickly to the surface. In isolation, a shift to smaller particles would therefore ultimately lead to greater surface nutrient supply and larger export rates (Fig. 2a, blue arrow), represented by the positive slope of the blue export-versus-β line in Fig. 2d. In the presence of this sinking speed effect (SSE), changes in export and β under slowed circulation must fall along the blue sinking speed-related export-versus-β line (Fig. 2d). In the absence of this sinking speed effect (i.e., particle size does not affect sinking rates/remineralization depths), there is no such requirement, and the initial stratification-induced export decrease would remain unaltered ("SC without SSE, with EE" point in Fig. 2d).

Only in the presence of both the ecological and sinking speed effects will the PSR feedback function; in this case, after circulation is slowed, export and β must reach a new steady-state at the intersection of the red and blue lines ("SC with SSE *and* EE" yellow star in Fig. 2d). Thus, the overall decrease in POC export would be smaller than predicted from decreased circulation rates and surface nutrient supply alone. That is, the net effect of phytoplankton

https://doi.org/10.5194/bg-2020-156
Preprint. Discussion started: 25 May 2020


Biogeosciences Discussions Open Access EGU

selection and particle size-dependent remineralization depths provides a negative feedback on, or dampening of, changes in export. Though the above description focuses on export decreases under decreased circulation rates, the PSR feedback would result in an analogous dampening of export increases under increased circulation rates and surface nutrient supply.

To quantify the strength of this hypothesized feedback, we employ a 3-D global ocean biogeochemical model and remotely-sensed estimates of carbon export and particle size distributions. To isolate the effects of the feedback, we take an idealized approach using empirical relationships and a simple model that allows responses to be easily traced back to assumptions made at each step. In doing so, we produce a first-order estimate of the particle size-remineralization (PSR) feedback strength throughout the ocean.

2 Methods

2.1 Ocean biogeochemical and particle remineralization model

2.1.1 Model setup

We examine the PSR feedback within the context of an idealized ocean biogeochemical model, which comprises a simple nutrient cycle (DeVries et al., 2014) embedded within the Ocean Circulation Inverse Model (OCIM) (DeVries, 2014). OCIM assimilates passive and transient tracer observations to constrain the time-mean, large-scale circulation at 2-degree horizontal resolution on 24 vertical layers. Nutrient cycling comprises phosphate (PO_4^{3-}) uptake and export in the surface ocean (<75m), particle remineralization in the subsurface (>75m), and production and decomposition of dissolved organic phosphorus.

Remineralization is represented implicitly based on the attenuation of the particle flux, as predicted by the 1-D mechanistic Particle Remineralization and Sinking Model (PRiSM). PRiSM computes particle flux profiles as a function of particle size distribution (β) at the surface, microbial remineralization rates, and physical relationships between particle size, mass, and sinking velocity. Using PRiSM, variations in annual mean β of the magnitude observed by satellite can lead to large differences in particle fluxes at depth (Fig. S1; Fig. 1a,d; DeVries et al 2014). Model configuration and parameter values used here are listed in Table S1; further model details and validation are described in DeVries et al. (2014). Here we extend the original PRiSM-enabled biogeochemical model in two important ways:

1. We add the ability to enable or disable the PSR feedback by optionally allowing the particle size distribution to respond to changes in nutrient supply (Section 2.1.2).
2. The original diagnostic nutrient uptake term (i.e., nutrient-restoring production) is replaced by the prognostic organic matter production scheme developed by Weber and Deutsch (2012) with minor parameter updates (see Table S2). This scheme calculates phytoplankton growth rates as a function of observed annual-mean temperatures (Locarnini et al., 2010) and solar radiation levels (Rossow & Schiffer, 1999), along with modeled PO_4^{3-}. We thus explicitly model phytoplankton production in terms of phosphorus consumption and regeneration. We then use an empirical, spatially variable relationship between particulate C-to-P ratios and

https://doi.org/10.5194/bg-2020-156
Preprint. Discussion started: 25 May 2020


Biogeosciences Discussions Open Access EGU

phosphate concentrations (Galbraith & Martiny, 2015) to convert phytoplankton production into units of carbon. It is assumed that 10% of phytoplankton production is routed directly to dissolved organic matter in the euphotic zone, with the remainder becoming particulate organic matter (Thornton, 2013).

2.1.2 Model representation of the PSR feedback

When the PSR feedback is disabled within our model, nutrient supply changes drive changes in export, but β remains constant over time. With the PSR feedback enabled, nutrient supply changes drive changes in export *and* β via an empirically-derived, spatially variable relationship between export and β that is detailed in Section 2.2. In this way, β can respond dynamically to a change in nutrient supply, leading to changes in remineralization depth, and initiating the feedback described in Section 1.2. Mathematically, β is updated at a given grid point as follows between timesteps t and $t+1$:

$$\beta_{t+1} = \beta_t + \frac{d\beta_{obs}}{dE_{n,obs}} \frac{E_{t+1}-E_t}{E_t}, \quad (1)$$

where E is model-derived export and $\frac{d\beta_{obs}}{dE_{n,obs}}$ is the empirically-derived, time-independent fractional change in observed β (β_{obs}) per change in observed time-mean normalized export ($E_{n,obs}$) (i.e., absolute export divided by time-mean export at a given grid point).

To disable the feedback, $\frac{d\beta_{obs}}{dE_{n,obs}}$ is set equal to zero so that modeled β remains constant over time. To enable the feedback, $\frac{d\beta_{obs}}{dE_{n,obs}}$ is set equal to the linear temporal regression coefficient between β_{obs} and $E_{n,obs}$, which is computed from remotely-sensed time series of the two variables over the global ocean (Section 2.2). Thus, when the feedback is enabled, changes in modeled β over time are dictated by the magnitude of modeled export change as well as the strength of the relationship between observed β and export, which can vary spatially.

2.2 Empirical analyses of phytoplankton size, β, and export from satellite data

Because the strength of our modeled PSR feedback depends strongly on the observed relationship between β and export ($\frac{d\beta_{obs}}{dE_{n,obs}}$ in Eq. (1)), we sought a robust empirical constraint on this relationship. Sections 2.2.1 and 2.2.2 respectively describe the global satellite-derived time series maps of β and export used here. Section 2.2.3 then describes how these monthly-mean β and export maps are used to compute a range of possible global $\frac{d\beta_{obs}}{dE_{n,obs}}$ relationships.

2.2.1 Global satellite-derived particle size distribution map

Global 1/12°-by-1/12° monthly maps of β observed by the SeaWiFS satellite sensor (in operation from September 1997 – December 2010) were downloaded from ftp://ftp.oceancolor.ucsb.edu//pub/org/oceancolor/MEaSUREs/PSD/. These β maps were derived from remotely-sensed particulate backscatter validated with in situ near-surface Coulter counter measurements (Kostadinov et al.,

https://doi.org/10.5194/bg-2020-156
Preprint. Discussion started: 25 May 2020

2009). To enable more efficient computation, we reduced the resolution of the original monthly β maps to 1°-by-1° degree via spatial averaging. At this resolution, time-mean β ranges from ~3.3 in coastal high-latitude regions (where high nutrient conditions favor larger phytoplankton) to ~5.3 in the subtropics (where low macronutrient concentrations favor small phytoplankton) (Fig. 1a).

2.2.2 Global satellite-derived export maps

Export is computed here as the product of net primary production (NPP) and the particle export ratio (export/NPP, or e-ratio), both of which can be derived from satellite. To create a range of plausible global monthly export maps, we multiplied all possible permutations of three monthly NPP and e-ratio maps, yielding nine distinct monthly time series of global export (Fig. S2). All three sets of monthly satellite NPP maps were downloaded from http://sites.science.oregonstate.edu/ocean.productivity/ and derived from SeaWiFS observations processed through the following algorithms: (i) the chlorophyll-based Vertically Generalized Production Model (VGPM) (Behrenfeld & Falkowski, 1997); (ii) the Eppley-VGPM model (VGPME), containing a modified relationship between temperature and production compared to the original VGPM (Carr et al., 2006); and (iii) the Carbon-based Production Model (CbPM), which uses particulate backscatter-derived carbon rather than chlorophyll to measure phytoplankton biomass (Behrenfeld et al., 2005). The three sets of monthly-mean e-ratio maps were computed from empirical relationships derived by L2000 (Laws et al., 2000), D2005 (Dunne et al., 2005), and L2011 (Laws et al., 2011). L2000 computes e-ratios from SST alone; D2005 computes e-ratios from NPP, SST, and euphotic zone depths; and L2011 computes e-ratios from SST and NPP. The in situ, statistically interpolated SST dataset used here was NOAA's Extended Reconstructed Sea Surface Temperature (ERSST) v3b, downloaded from https://www1.ncdc.noaa.gov/pub/data/cmb/ersst/v3b/netcdf/ (Smith et al., 2008). Euphotic zone depths needed to compute D2005 e-ratios were derived from SeaWiFS-sensed chlorophyll concentrations (downloaded from the same website as NPP) according to Equation 10 in Lee et al. (2007). As with β, all variables were computed and stored on a 1°-by-1° degree grid over the entirety of the SeaWiFS period (September 1997 – December 2010, 160 months long).

In the following analyses (Section 3), we employ all nine sets of global monthly export maps to propagate uncertainty in our results. When reporting most-likely values, we weight the nine map sets according to how well each map set's annual mean export matches in situ observations within each region defined here (Table S3; see Weber et al. (2016) for derivation of weighting factors). Fig. 3 shows the weighted annual mean carbon export flux over the nine map sets, as well as the regions used for weighting, which are delineated based on biogeochemical characteristics such as sea surface temperature and surface phosphate concentrations (Weber et al., 2016). The Atlantic and Pacific Oceans are divided into warm subtropics dominated by smaller picophytoplankton (STA, STP), cold subarctic regions dominated by blooms of larger microphytoplankton in the north (NA, NP), and cool tropical upwelling zones dominated by larger phytoplankton in the east (ETA, ETP). The Indian Ocean is kept intact (IND), while the Southern Ocean is divided into the productive, diatom-dominated Subantarctic Zone (SAZ) and the high-nutrient, low-chlorophyll Antarctic Zone (AAZ). The Indian Ocean region (IND) did not contain a sufficient number of in situ observations of export to enable comparison to the satellite export maps, so all nine maps are weighted equally there.

https://doi.org/10.5194/bg-2020-156
Preprint. Discussion started: 25 May 2020


Biogeosciences Discussions Open Access EGU

2.2.3 Regionally variable empirical β versus export relationships ($\frac{d\beta_{obs}}{dE_{n,obs}}$)

We quantify the empirical relationship between β and export individually for each grid cell by extracting the monthly timeseries of β and normalized export (E_n) from the satellite products described above, and then applying linear regression. This process produces a spatially variable, 1°-by-1° degree global map of the best-fit linear slopes ($\frac{d\beta_{obs}}{dE_{n,obs}}$) relating β and E_n. To capture the range of plausible $\frac{d\beta_{obs}}{dE_{n,obs}}$ maps, we repeat this process for each of the nine export products to generate nine distinct global $\frac{d\beta_{obs}}{dE_{n,obs}}$ maps (Fig. S3). To smooth out small-scale noise and illuminate larger-scale relationships, we then spatially average the slopes in each of the nine $\frac{d\beta_{obs}}{dE_{n,obs}}$ maps over the ocean biogeochemical regions defined in Fig. 3 (Fig. 4a). Lastly, we set the slopes at all grid points within a given region equal to that region's weighted (Table S3; Section 2.2.2) mean value (Fig. 4b) to generate the final $\frac{d\beta_{obs}}{dE_{n,obs}}$ map used in our PSR feedback-on runs (Fig. 4c).

To quantify the sensitivity of $\frac{d\beta_{obs}}{dE_{n,obs}}$ to the choice of export map used, we computed upper and lower-bound $\frac{d\beta_{obs}}{dE_{n,obs}}$ maps by adding and subtracting one standard deviation (error bars in Fig. 4b) to the weighted regional mean $\frac{d\beta_{obs}}{dE_{n,obs}}$ values. Conducting PSR feedback-on runs using upper and lower-bound $\frac{d\beta_{obs}}{dE_{n,obs}}$ maps establishes the range of PSR feedback strengths we can reasonably expect from our model forced with empirically-derived relationships.

2.3 Model runs to simulate future ocean warming and quantify the PSR feedback effect

To represent present-day conditions, we run a baseline simulation with modern-day circulation rates to steady-state. To simulate increased water column stratification and reduced vertical exchange due to warming, we uniformly and instantaneously reduce circulation and diffusion rates by 10% throughout the ocean. For comparison, observations show that the Atlantic meridional overturning circulation (AMOC) has weakened by about 15% since the mid-20th century due to anthropogenic warming (Caesar et al., 2018), while ESMs project that AMOC will weaken by 11-34% over the 21st century, depending on the chosen radiative forcing scenario (11% assumes the "high mitigation" RCP2.6 scenario, while 34% assumes the "business-as-usual" RCP8.5 scenario) (Collins et al., 2019). A 10% decrease in circulation rates is therefore a relatively conservative estimate of the effects of anthropogenic warming. Although modulation of ocean circulation rates in response to climate change will be more complicated and variable than the uniform 10% decrease applied here (e.g., Toggweiler and Russell, 2008), we seek only a simple, idealized way to approximate the reduced surface nutrient supply that is expected in a warmer future ocean.

To quantify the impact of the global PSR feedback on export changes with future warming, we run the slower-circulation rate simulation with and without the PSR feedback effect enabled. In feedback-off runs, β is set equal to annual mean values (Fig. 1a) for the entire duration of the run. In feedback-on runs, β is initially set equal to annual mean values, but is allowed to change according to Eq. (1), with $\frac{d\beta_{obs}}{dE_{n,obs}}$ defined as in Fig. 4c for the entire duration of

https://doi.org/10.5194/bg-2020-156
Preprint. Discussion started: 25 May 2020


Biogeosciences Discussions Open Access EGU

the run. Additional feedback-on runs were conducted using the upper and lower-bound $\frac{d\beta_{obs}}{dE_{n,obs}}$ maps (described in Section 2.2.3).

All of the above described runs were also repeated with 10% faster circulation rates to determine whether the PSR feedback strength is symmetrical with regard to the direction of circulation change. Within all runs, β is constrained to realistically remain between 2 and 6.5 at all grid points, though these extremes are rarely reached. We run all experimental simulations for 100 years (initializing with conditions from the end of the present-day spin-up) to study near-future changes in export production and nutrient distributions, and to facilitate comparison with 100-year changes projected by the state-of-the-art Earth System Models discussed above.

3 Results and Discussion

3.1 Spatial patterns in empirically-derived β versus export relationships ($\frac{d\beta_{obs}}{dE_{n,obs}}$)

No matter which maps are used (Section 2.2), satellite-derived β and export are strongly negatively correlated. Export thus tends to be high when β is small (particles are large) and low when β is large (particles are small) (Fig. 4; Fig. S3), as hypothesized in Section 1.2 and highlighted by the negatively-sloped red "Ecological Effect" line in Fig. 2c-d. Regions that are more nutrient-limited (i.e., the subtropics) exhibit especially strong negative relationships between β and export (Fig. 4; Fig. S3), as both β and export are predominantly driven (in opposite directions) by surface nutrient supply in these areas. The counterintuitive weakly positive relationship between β and export in the SAZ is in line with findings from Lam and Bishop (2007), who showed that in the Southern Ocean, areas with higher biomass and larger particles at the surface were actually associated with lower rates of export out of the euphotic zone and at 200 m depth. In these diatom-dominated regions, zooplankton may be more active and have higher particle grazing efficiencies, leading to faster attenuation of particulate carbon fluxes with depth. The unique relationship between β and export in the SAZ and potentially the Southern Ocean at large is worth further exploration outside of this study.

3.2 Predicted export changes in the presence of the global PSR feedback effect

In this section, we discuss differences in predicted export production changes under altered circulation rates with and without the PSR feedback effect applied globally. Sections 3.2.1 and 3.2.2/3.2.3 respectively examine resultant global and zonal/regional mean changes in export.

3.2.1 Predicted global mean export changes with and without the global PSR feedback

To examine the global strength of the PSR feedback within our model under climate change conditions, we compare global mean export changes over time in the PSR feedback-on and off runs after a 10% decrease in circulation rates (Fig. 5, comparing slower circulation dashed and solid lines). In both the feedback-on and off cases, instantaneously decreasing circulation rates reduces surface nutrient supply and immediately leads to a sharp decrease

https://doi.org/10.5194/bg-2020-156
Preprint. Discussion started: 25 May 2020

in global mean export of ~0.2 molC m^{-2} yr^{-1} from 3.54 molC m^{-2} yr^{-1}. After this initial plunge, global mean export declines by an additional 0.09 molC m^{-2} yr^{-1} over the next 100 years with the feedback off (for a total decrease of 0.29 molC m^{-2} yr^{-1} or 8.1%), versus an additional 0.05 molC m^{-2} yr^{-1} with the feedback on (for a total decrease of 0.25 molC m^{-2} yr^{-1} or 7.0%) (Fig. 5, slower circulation lines and bars). ESMs without the PSR feedback effect project global mean export decreases of around 7-18% between 2090-2099 and 1990-1999 under a "business-as-usual" radiative forcing scenario (RCP8.5). In the absence of the PSR feedback, the 100-year global mean export decrease of 8.1% predicted by our model is comparable to, but on the low-end of, these ESM projections, likely because of the conservative 10% decrease in circulation rates applied here.

Turning the PSR feedback on in our model reduced the total 100-year predicted decrease in export by ~14% (visually, the ratio of the solid-colored bar length to the full bar length below zero in Fig. 5). At equilibrium (when global mean export stabilizes ~500 years after decreasing circulation rates), this feedback effect increases to ~16%. With the feedback turned on, particle sizes shrink and remineralization depths shoal in response to an initial circulation-driven decrease in surface nutrient supply, thereby moderating this initial decrease by keeping more recycled nutrients at the surface. In particular, global mean β increases by 0.03 units (from 4.34 to 4.37) under 10% decreased circulation rates after 100 years with the PSR feedback on (Fig. 6a,b), corresponding to a 17 m global mean shoaling (from 595 to 578 m) of e-folding remineralization depths (Fig. 6b). The greatest regional mean β increase of 0.06 occurs in the Indian Ocean (IND), resulting in a 41 m shoaling of remineralization depths there (Fig. 6b). Results from runs employing upper and lower-bound $\frac{d\beta_{obs}}{dE_{n,obs}}$ maps (defined in Section 2.2.3, represented by the error bars in Fig. 4b) lend further support to our findings and indicate that the modeled global PSR feedback effect size is relatively insensitive to the choice of export maps used to compute $\frac{d\beta_{obs}}{dE_{n,obs}}$ (Fig 5, black error bars).

The PSR feedback also dampens the response of global-mean carbon export to an instantaneous *increase* in ocean circulation rates (Fig. 5). One hundred years after circulation rates are increased by 10%, global mean carbon export increases from 3.54 molC m^{-2} yr^{-1} by 0.28 molC m^{-2} yr^{-1} (8.0%) with the feedback off, whereas it increases by ~0.23 molC m^{-2} yr^{-1} (6.6%) with the feedback on (Fig. 5, faster circulation lines and bars). Thus increasing circulation rates by 10% with the PSR feedback on reduces the 100-year increase in export production by ~18% (visually, the ratio of the solid-colored bar length to the full bar length above zero in Fig. 5). At equilibrium, this feedback effect increases to ~20%. With the feedback turned on, particle sizes grow and remineralization depths deepen in response to an initial circulation-driven increase in surface nutrient supply, thereby moderating this initial increase by transferring more nutrients to deeper waters where they recirculate more slowly to the surface. In particular, global mean β decreases by 0.03 units (from 4.34 to 4.31) under 10% increased circulation rates, corresponding to a 20 m global mean deepening (from 595 to 615 m) of e-folding remineralization depths (not shown). The greatest regional mean β decrease of 0.07 occurs in the Indian Ocean (IND), resulting in a 54 m shoaling of remineralization depths there. Compared with the decreased circulation case, absolute changes in remineralization depths are slightly larger under increased circulation rates because remineralization depth changes are more sensitive to variations in β when particles are larger (that is, at smaller values of β). Because remineralization depth changes are greater under increased

https://doi.org/10.5194/bg-2020-156
Preprint. Discussion started: 25 May 2020


Biogeosciences Discussions Open Access EGU

circulation rates, so too is the global PSR feedback strength (14% with decreased circulation rates versus 18% with increased circulation rates). Again, results from PSR feedback-on runs constrained by upper and lower-bound $\frac{d\beta_{obs}}{dE_{n,obs}}$ maps further support the notion that the PSR feedback size is relatively insensitive to the choice of export maps used to compute $\frac{d\beta_{obs}}{dE_{n,obs}}$ (Fig 5, error bars). Thus, the effect of the PSR feedback is to buffer changes in export production in response to any physical perturbation in nutrient supply, regardless of the direction.

3.2.2 Predicted zonal and regional mean export changes *without* the global PSR feedback

In our baseline simulation under current-day circulation rates, POC export covaries tightly throughout the low to mid-latitudes with nutrient concentrations in shallow subsurface waters beneath the euphotic zone, quantified here as [PO_4] at 200m depth (P_{200m}) (Fig. 7a,b; Fig. 8a). South of ~40°S and north of ~40°N, other factors such as light and/or temperature become limiting; as a result, export does not vary as tightly with P_{200m} in these higher-latitude regions. The spatial structure of the relationship between export and P_{200m} confirms that nutrient supply from subsurface layers is the primary driver of export rates throughout the nutrient-limited low- to mid-latitudes. Therefore, in these regions, the following balance approximately holds:

$$Export = E \approx wP_{200m}, \quad (2)$$

where w is the local upwards nutrient supply velocity, which represents the net effect of all vertical exchange processes, including diffusion, upwelling, entrainment, and mixing. This balance can in turn be used to derive a simple diagnostic for understanding changes in export under altered circulation rates at any given location:

$$\Delta E = \Delta w * P_{200m,baseline} + w_{baseline} * \Delta P_{200m}, \quad (3)$$

where *baseline* denotes variables from the baseline simulation ran to steady-state with current-day circulation rates and Δ denotes change from the baseline simulation under altered circulation rates. (Note that we ignore the "perturbation product" term, $\Delta w * \Delta P_{200m}$, because it is negligible.) When ocean circulation is slowed, Eq. (3) allows us to identify two different contributions to the resultant reduction in export through the low to mid-latitudes. First, and most intuitively, when circulation rates are uniformly decreased, w is reduced across the entire ocean ($\Delta w < 0$) and the supply of "baseline" nutrients is curtailed. Second, a decrease in circulation rates also reduces phosphate concentrations throughout the shallow subsurface layer in the low to mid-latitudes ($\Delta P_{200m} < 0$) (solid lines and bars in Fig 7c,d; Fig. 8b). This decrease in P_{200m} is largely driven by enhanced biological nutrient utilization in the surface of the Southern Ocean in response to slower circulation, which is then propagated into the low to mid-latitude interior through Antarctic Intermediate and Subantarctic Mode Waters, as observed in future climate simulations by more complex ESMs (e.g., Moore et al., 2018).

Together, the decreases in shallow subsurface nutrient concentrations (P_{200m}) and vertical exchange rates (w) result in substantial reductions in export throughout most of the ocean under our decreased circulation simulations as dictated by Eq. (3), with the greatest reductions occurring in nutrient-limited areas. In the absence of the PSR feedback, the 10% decrease we imposed on circulation rates leads to 100-year zonal mean export decreases of >15% at 35°N and S and ~10% between 35°N and S (solid line in Fig. 7e). Regionally, the oligotrophic subtropics (especially the

https://doi.org/10.5194/bg-2020-156
Preprint. Discussion started: 25 May 2020


Biogeosciences Discussions Open Access EGU

STP) exhibit the largest relative decreases in export (~10-13%), followed closely by the tropics (ETA, ETP) with export decreases around 8-10% (solid bars in Fig. 7f). As expected, the decrease in export mirrors the pattern of ΔP_{200m} in low to mid-latitude regions due to a strong dependence of export on nutrient supply from the shallow subsurface here.

3.2.3 Predicted zonal and regional mean export changes *with* the global PSR feedback

As with the global mean (Section 3.2.1), we quantify zonal and regional mean PSR feedback strength as the difference in circulation-driven export change from baseline between the feedback-on and -off runs, normalized by the change from baseline in the feedback-off run. In other words, the PSR feedback strength is the percentage by which turning on the PSR feedback reduces (dampens) the response of carbon export to changes in ocean circulation (blue line and bars in Fig. 7g,h). Visually, the zonal mean feedback strength (blue line in Fig. 7g) is equal to the difference between the dashed and solid lines divided by the solid line in Fig. 7e, while the regional mean PSR feedback strength (blue bars in Fig. 7h) is equal to the length of the solid-colored portion of the bars divided by the entire length of the bars in Fig. 7f. The PSR feedback strength is greatest (most strongly damping) in the low to mid-latitudes and in the tropics (ETA, ETP) and subtropics (STA, STP, IND), with the feedback able to reduce zonal and regional mean export changes by up to 20% in these regions (blue lines and bars in Fig. 7g,h). To understand this spatial pattern, we combine Eq. (3) with our definition of PSR feedback strength to yield the following diagnostic:

$$PSR\ feedback\ strength = \frac{\Delta E_{on} - \Delta E_{off}}{\Delta E_{off}} \approx \frac{\frac{\Delta P_{200m,on} - \Delta P_{200m,off}}{P_{200m,baseline}}}{\frac{\Delta w}{w_{baseline}} + \frac{\Delta P_{200m,off}}{P_{200m,baseline}}}, \quad (4)$$

where *on/off* denotes whether the PSR feedback was turned on or off under the altered circulation rates. This expression reveals that the PSR feedback effect is strongest wherever activating the feedback leads to the greatest dampening of changes in P_{200m}, compared to the changes that occur in the feedback-off case. In the decreased circulation simulations ($\frac{\Delta w}{w_{baseline}}$ = -10% everywhere), the low to mid-latitude regions display the greatest differences in P_{200m} changes between feedback-on and off runs (Fig. 7c,d; Fig. 8b-d); these regions undergo the greatest reductions in circulation-driven export change due to the PSR feedback (Fig. 7e,f) and thus exhibit the largest PSR feedback effects (blue lines and bars in Fig. 7g,h).

The degree to which the PSR feedback dampens P_{200m} changes is in turn driven by the strength of the relationship between β and export. The low to mid-latitudes exhibit the most negative $\frac{d\beta_{obs}}{dE_{n,obs}}$ values and therefore, the tightest coupling between β and export (Fig. 4c). In these regions, where macronutrient limitation is the dominant constraint on productivity, a given circulation-driven decrease in surface nutrient supply causes a relatively large drop in both export and phytoplankton/particle size (leading to an increase in β) in the presence of the PSR feedback. This then allows significantly more nutrients to be recycled at the surface, resulting in greatly dampened decreases in P_{200m} and subsequent export production.

Our simple diagnostic (Eq. (4)) can explain PSR feedback strengths quite well over the global ocean, as seen by comparing total feedback strengths (blue lines/bars in Fig. 7g,h) with the approximation based on w and P_{200m}

https://doi.org/10.5194/bg-2020-156
Preprint. Discussion started: 25 May 2020

(right-hand side of Eq. (4), represented by orange lines/bars in Fig. 7g,h). However, because new production can be fed by local upwelling as well as lateral advection, changes in P_{200m} and vertical exchange rates alone (orange lines/bars in Fig. 7g,h) cannot perfectly predict all changes in export (blue lines/bars in Fig. 7g,h), especially in regions where lateral advection plays a relatively large role in supplying nutrients to the surface (i.e., recall that Eq. (2) is only a close approximation).

3.3 Predicted export changes in the presence of regional PSR feedback effects

In this section, we discuss each individual ocean region's contribution to the global PSR feedback effect. To isolate the PSR feedback effect coming from each region, we conduct a set of model runs in which we decrease the circulation rate globally, but only activate the PSR feedback within one region at a time. In these feedback-on runs, we set $\frac{d\beta_{obs}}{dE_{n,obs}}$ in Eq. (1) equal to zero at all grid points outside of the region we are isolating; within the isolated region, we set $\frac{d\beta_{obs}}{dE_{n,obs}}$ equal to the corresponding empirically-derived value (as shown in Fig. 4b). These simulations are then compared to the same feedback-off run discussed in Section 3.2 (i.e., no changes in β anywhere) to determine the impact of enabling the feedback within one region at a time. Sections 3.3.1. and 3.3.2 respectively describe the global and regional mean export changes resulting from this set of experiments.

3.3.1 Predicted global mean export changes with and without regional PSR feedbacks

Analysis of the regional feedback-on runs show that tropical (ETA, ETP) and subtropical (STA, STP, IND) regions contribute most significantly to the global PSR feedback (Fig. 9). Turning the feedback on in the ETP alone, for instance, leads to a 3.9% reduction in global mean export change compared to the feedback-off case (Fig. 9a – row 7, last column); the ETP alone thus accounts for 38.6% of the global PSR feedback strength (Fig. 9b – row 7, last column), while spanning only 10.3% of total ocean area. Turning the feedback on in the subtropical (STA, STP, IND) and tropical (ETA, ETP) regions one at a time and then summing their individual contributions (11.7%, 11.6%, 22.3%, 13.3%, 38.6% respectively; Fig. 9b – last column) accounts for 97.5% of the global PSR feedback effect, while all other regions (AAZ, SAZ, NA, NP) account for only a negligible fraction of the effect (or even act to decrease the overall effect in the case of the SAZ) (Fig. 9b – last column). The dominant contributions of the tropical/subtropical regions to the global PSR feedback can once again be understood via spatial patterns in $\frac{d\beta_{obs}}{dE_{n,obs}}$ (Fig. 4c), with large changes in β and remineralization depth associated with relatively small changes in export in the nutrient-limited tropical/subtropical regions.

3.3.2 Predicted regional mean export changes with and without regional PSR feedbacks

The significant tropical/subtropical contribution to the PSR feedback can also be seen by examining export changes within individual regions. Activating the PSR feedback in the STA, for example, dampens regional mean export decreases within the STA, the ETA, and the NA by 7.7%, 3.1%, and 2.2%, respectively (Fig. 9a – row 3). Turning on the feedback in the STP (Fig. 9a – row 4), ETA (Fig. 9a – row 6), or ETP (Fig. 9a – row 7) alone have

https://doi.org/10.5194/bg-2020-156
Preprint. Discussion started: 25 May 2020


Biogeosciences Discussions Open Access EGU

similarly large effects on surrounding regions. In contrast, activating the feedback within higher-latitude regions (AAZ, SAZ, NA, NP) neither significantly moderates export decreases in any individual regions nor globally (Fig. 9a – rows 1-2, 8-9). The AAZ uniquely undergoes near-zero decreases in export for all runs with the feedback on or off; PSR feedback strength here is therefore negligible (Fig. 9a,b – row 1).

When the PSR feedback is turned on within a given region, the effect is typically felt most strongly within that same region, as would reasonably be expected given that export production and resultant remineralization are spatially co-occurring (Fig. 9a,b – diagonal going from upper left to lower right corner). However, depending on the local magnitude of $\frac{d\beta_{obs}}{dE_{n,obs}}$ compared to that of neighboring regions, as well as the connectivity of nutrient supplies between them, there can be substantial PSR feedback effects originating from afar. For example, in the Pacific basin, switching on the PSR feedback in the ETP has a stronger buffering effect on export in the STP region than switching on the feedback in the STP itself (Fig. 9b – row 7, column 4). This is because the relationship between β and export is much stronger in the ETP (with a regional mean $\frac{d\beta_{obs}}{dE_{n,obs}}$ of -0.40; see Fig. 4c) than in the STP (with a regional mean $\frac{d\beta_{obs}}{dE_{n,obs}}$ of -0.18; see Fig. 4c), and because remineralized surface nutrients in the ETP are readily carried into the STP by wind-driven Ekman transport. In this way, PSR feedback-driven buffering of surface nutrient supply changes within the ETP indirectly buffers surface nutrient supply changes in the STP as well. This indirect effect also operates in the reverse direction, in that activating the PSR feedback in the STP also has a relatively strong impact back on the ETP (Fig. 9b – row 4, column 7). In this case, nutrients remineralized shallower in the STP thermocline are directed along sloping isopycnals that eventually upwell into the ETP surface, thus buffering decreases in export there. The STP also has a relatively large PSR feedback effect on the subpolar NP (Fig. 9b – row 4, column 9), due to the intense flow of the Kuroshio Current, which carries surface nutrients from the STP northward.

Similar relationships hold in the Atlantic basin between the tropics, subtropics, and subpolar regions. However, the PSR feedback effect of the ETA on the STA is smaller (Fig. 9b – row 6, column 3), while the effect of the STA on the ETA is larger (Fig. 9b – row 3, column 6) compared to their Pacific counterparts, presumably due to less pronounced Ekman divergence along the equatorial Atlantic. The STA's PSR feedback effect on the subpolar NA (Fig. 9b – row 3, column 8) is also substantially more pronounced than the STP's effect on the NP, indicating a stronger nutrient supply pathway between subtropical and subpolar gyres in the Atlantic Ocean via the Gulf Stream.

An interesting phenomenon that arises in the Southern Ocean is the negative (dampening) overall PSR feedback effect on the SAZ (Fig. 9a – row 10, column 2), despite a positive (amplifying) local feedback effect (Fig. 9a,b – row 2, column 2) and relationship between β and export here (regional mean $\frac{d\beta_{obs}}{dE_{n,obs}}$ of +0.13; see Fig. 4c). Additive negative (dampening) PSR feedback effects from surrounding regions (STA, STP, IND, ETA, ETP) (Fig. 9a,b – rows 3-7, column 2) overcome the small positive (amplifying) local feedback effect here (Fig. 9a,b – row 2, column 2), such that the total feedback effect still reduces the magnitude of the regional mean export decrease by 1.2% compared to the feedback-off case (Fig. 9a – last row, column 2). Because the SAZ spans the entire width of the ocean and touches every other basin, additional remineralized surface nutrients collected in the many connected

https://doi.org/10.5194/bg-2020-156
Preprint. Discussion started: 25 May 2020

466 regions are quickly and easily circulated into the SAZ when the global PSR feedback is active, thus buffering larger
467 would-be decreases in export here.

468 **4 Conclusion**

469 Surface nutrient supply drives export production and shapes phytoplankton communities and particle size
470 distributions throughout the low to mid-latitude oceans. Large phytoplankton and particles are prevalent in nutrient
471 replete conditions, while smaller phytoplankton and particles dominate in oligotrophic conditions (Litchman et al.,
472 2007; Guidi et al., 2007; 2008; 2009). A reduction in surface nutrient supply stemming from increased water column
473 stratification in a warming ocean (Bopp et al., 2013; Cabré et al., 2015a; Capotondi et al., 2012) thus leads to a decrease
474 in global export production (Fig 2, green arrows; Fig. 5, slower circulation solid lines/bars) *and* sinking particle size
475 (Fig 2a, red arrow; Fig. 2c-d, red line; Fig. 6b). Smaller particles in turn drive shallower nutrient remineralization and
476 thus faster resupply of those nutrients to the surface, dampening the initial circulation-driven change in export (Fig.
477 2a, blue arrow; Fig. 2d, blue line; Fig. 5, slower circulation dashed lines/hatched bars; Fig. 6b; Fig. 7c-f; Fig. 8b-c).
478 This study has shown that these mechanisms can give rise to a negative feedback loop that moderates the response of
479 carbon export to changes in ocean circulation, which we term the particle size-remineralization (PSR) feedback.
480 Many global models ignore the effects of nutrient supply on particle size and/or the effects of particle size
481 on remineralization depths (Laufkötter et al., 2016 and references therein). Within our model, including these effects
482 reduces the magnitude of predicted 100-year changes in global export production by ~14% when circulation rates are
483 decreased by a conservative 10% (Fig. 5). This implies that global models without the PSR feedback may be
484 overestimating 100-year climate-driven export decreases by ~1.16 times. Under a relatively extreme ESM-projected
485 decrease of 18% by 2100 (Bopp et al., 2013), absolute global export would be reduced by ~0.7-2.9 GtC/yr, assuming
486 a present rate in the range of 4-16 GtC/yr (Boyd & Trull, 2007; DeVries & Weber, 2017; Dunne et al., 2005, 2007;
487 Falkowski et al., 1998; Henson et al., 2011; Laws et al., 2000; Siegel et al., 2014; Yamanaka & Tajika, 1996); with
488 the PSR feedback in effect, this predicted decrease would be reduced by ~14% to ~0.6-2.3 GtC/yr.
489 The PSR feedback is strongest (moderating export changes by up to 20%; Fig. 7g,h; Fig. 9) and export
490 decreases are thus likely to be most overestimated in the low-latitude tropical and subtropical regions, where current
491 models also predict some of the largest future export decreases (Bopp et al., 2013; Cabré et al., 2015a). Within these
492 regions, primary and export production are highly nutrient-limited, such that a given stratification-induced decrease
493 in nutrient supply leads to relatively large decreases in export and sinking particle size (Fig. 4), with correspondingly
494 large effects on remineralization depth (Fig. 6) and surface nutrient recycling. Because these regions exhibit the
495 greatest projected decreases in export as well as the strongest PSR feedback effects, spatial variations in projected
496 export decrease may also be less pronounced than currently expected.
497 The PSR feedback operates on increases in surface nutrient supply as well. Under surface nutrient supply
498 increases, phytoplankton/particles grow larger and remineralization depths deepen, which sends more nutrients out of
499 the shallow subsurface and thereby moderates initial circulation-driven increases in export. This PSR feedback reduces
500 the magnitude of predicted 100-year changes in global export production by about 18% when circulation rates are

https://doi.org/10.5194/bg-2020-156
Preprint. Discussion started: 25 May 2020

increased by 10% (Fig. 5, faster circulation dashed lines/hatched bars). In scenarios of global cooling (resulting in water column destratification, enhanced mixing, and increased surface nutrient supply), centennial-scale projections of export increase in models lacking the PSR feedback would therefore be >1.2 times too big, again with the largest overestimates in the low to mid-latitude regions. The PSR feedback thus moderates export changes in response to any physical perturbation to surface nutrient supply, whether driven by increasing or decreasing circulation rates. Of particular note, the strength of the PSR feedback does not depend on the size of circulation rate changes (i.e., PSR feedback strength remains relatively constant whether circulation rates are increased/decreased by 10% or 50% - results not shown).

The exact strength of the PSR feedback hinges on the empirical relationship between carbon export and particle size, which may differ depending on the datasets used to constrain it. To address this uncertainty, we correlated β against a range of different global export datasets and found that our results were relatively insensitive to the choice of export dataset. Unfortunately, well-grounded alternative global and temporally-resolved datasets for β were not readily available, so uncertainty in the PSR feedback strength due to uncertainties in observed β could not be quantified here. Analysis of in situ Underwater Visual Profiler (UVP) data suggests that β may actually be smaller (thus particles, larger) and less variable (Cram et al., 2018) than the backscatter-derived values (Kostadinov et al., 2009) used in this study. This would potentially imply less variability in particle size-driven remineralization depths, weakening the PSR feedback strength calculated here. On the other hand, differences in remineralization depths are greater at smaller values of β (Fig. S1; Fig. 2 in Devries et al., 2014), such that any given increase in β associated with a decrease in export would lead to greater shoaling of remineralization depths and a larger PSR feedback effect than calculated here. More in situ observations of β are clearly needed to better resolve these competing effects. One potential explanation for these β discrepancies is that the algorithm used to derive β from remotely-sensed particulate backscatter sometimes misses the largest particles in high-productivity areas such as the Southern Ocean (Kostadinov et al., 2009). In addition to the theories proposed in Lam and Bishop (2007), this may partly explain why $\frac{d\beta_{obs}}{dE_{n,obs}}$ is weakly positive in the Subantarctic Zone (SAZ); particles may actually get larger with increasing export here, but because they are already quite large, the satellite β sensor/algorithm may not be able to capture the particles becoming any larger. The result would be an underestimation of the negative (dampening) PSR feedback effect in this region. Another caveat of our study is that very simple phytoplankton biology and growth dependent on only one macronutrient was assumed. Furthermore, explicit zooplankton and the effects of particle fragmentation via grazing (e.g. Cavan et al., 2017) or particle aggregation via fecal pellet production (e.g. Steinberg et al., 2012; Turner, 2015 and references therein) were not included. Despite the aforementioned shortcomings, the results presented here represent a reasonable first attempt to quantify the strength of the PSR feedback effect on export changes within a global model.

Future work should test the PSR feedback effect in more complex models that better resolve phytoplankton/zooplankton biology, particle dynamics, and/or circulation changes. These models could include particle aggregation-disaggregation with prognostic sinking speeds (Gehlen et al., 2006), empirically-driven food-webs (Siegel et al., 2014), explicit phytoplankton and grazers of different sizes (Buesseler & Boyd, 2009), and/or spatiotemporally-resolved circulation changes that respond directly to atmospheric forcing. Additionally, future work

https://doi.org/10.5194/bg-2020-156
Preprint. Discussion started: 25 May 2020

should analyze the downstream effects of the PSR feedback on climate-driven projections of fisheries productivity, dissolved oxygen availability, and carbon sequestration in the deep ocean over centennial to millennial timescales. A smaller-than-currently-projected decrease in surface nutrient supply and export rates would be beneficial for maintaining fisheries, for example, but perhaps detrimental for deep ocean carbon sequestration. In particular, a decrease in circulation rates should enable enhanced carbon sequestration, as nutrients and CO_2 collect in the deep ocean (Fig. 8), but the PSR feedback may potentially moderate this increased sequestration effect. Other remineralization depth-related feedbacks not studied here may also be important for modulation of future changes in carbon export and its downstream effects; these should be investigated in future work as well. For instance, temperature increases may speed up bacterial remineralization rates (Cavan et al., 2019; Cram et al., 2018; John et al., 2014; Marsay et al., 2015; Matsumoto, 2007) and enhance recycling of nutrients near the surface, which would result in an additional negative feedback on export acting in the same direction as the PSR feedback. Oxygen concentrations, on the other hand, are predicted to decrease with future warming (Bopp et al., 2002; Cabré et al., 2015b; Keeling et al., 2010; Long et al., 2016; Matear & Hirst, 2003; Schmidtko et al., 2017), resulting in depressed bacterial remineralization and zooplankton grazing rates (Cavan et al., 2017; Devol & Hartnett, 2001; Hartnett & Devol, 2003; Van Mooy et al., 2002), which would further exacerbate circulation-driven nutrient supply decreases in the surface ocean and create a positive feedback on export production changes. A decrease in mineral ballasting of sinking particles with ocean acidification may also feedback positively on export production decreases (Hofmann and Schellnhuber, 2009). Ensuring that the PSR and other remineralization feedbacks are adequately represented in ESMs should be a priority of the modeling community to enable robust predictions of carbon export fluxes in the future ocean.

Code availability

The MATLAB code required to make the figures generated here can be found at https://doi.org/10.5281/zenodo.3785725.

Data availability

Data in the form of *.mat files required to the make the figures generated here can be found at http://doi.org/10.5281/zenodo.3785724.

Author contribution

SL and CD designed the model experiments. SL developed the model code and performed the simulations. SL prepared the manuscript with contributions from all co-authors.

References

https://doi.org/10.5194/bg-2020-156
Preprint. Discussion started: 25 May 2020


Biogeosciences Discussions Open Access EGU

567 Alldredge, A. L. and Gotschalk, C.: In situ settling behavior of marine snow, Limnology and Oceanography, 33(3),
568 339–351, doi:10.4319/lo.1988.33.3.0339, 1988.
569 Aumont, O. and Bopp, L.: Globalizing results from ocean in situ iron fertilization studies, Global Biogeochemical
570 Cycles, 20(2), doi:10.1029/2005GB002591, 2006.
571 Bach, L. T., Boxhammer, T., Larsen, A., Hildebrandt, N., Schulz, K. G. and Riebesell, U.: Influence of plankton
572 community structure on the sinking velocity of marine aggregates, Global Biogeochemical Cycles, 30(8),
573 1145–1165, doi:10.1002/2016GB005372, 2016.
574 Behrenfeld, M. J. and Falkowski, P. G.: Photosynthetic rates derived from satellite-based chlorophyll concentration,
575 Limnology and Oceanography, 42(1), 1–20, doi:10.4319/lo.1997.42.1.0001, 1997.
576 Behrenfeld, M. J., Boss, E., Siegel, D. A. and Shea, D. M.: Carbon-based ocean productivity and phytoplankton
577 physiology from space, Global Biogeochemical Cycles, 19(1), doi:10.1029/2004GB002299, 2005.
578 Bopp, Monfray, P., Aumont, O., Dufresne, J.-L., Treut, H. L., Madec, G., Terray, L. and Orr, J. C.: Potential impact
579 of climate change on marine export production, Global Biogeochemical Cycles, 15(1), 81–99,
580 doi:10.1029/1999GB001256, 2001.
581 Bopp, Resplandy, L., Orr, J. C., Doney, S. C., Dunne, J. P., Gehlen, M., Halloran, P., Heinze, C., Ilyina, T., Séférian,
582 R., Tjiputra, J. and Vichi, M.: Multiple stressors of ocean ecosystems in the 21st century: projections with
583 CMIP5 models, Biogeosciences, 10(10), 6225–6245, doi:https://doi.org/10.5194/bg-10-6225-2013, 2013.
584 Bopp, L., Quéré, C. L., Heimann, M., Manning, A. C. and Monfray, P.: Climate-induced oceanic oxygen fluxes:
585 Implications for the contemporary carbon budget, Global Biogeochemical Cycles, 16(2), 6-1-6–13,
586 doi:10.1029/2001GB001445, 2002.
587 Bopp, L., Aumont, O., Cadule, P., Alvain, S. and Gehlen, M.: Response of diatoms distribution to global warming
588 and potential implications: A global model study, Geophysical Research Letters, 32(19),
589 doi:10.1029/2005GL023653, 2005.
590 Boss, E., Twardowski, M. S. and Herring, S.: Shape of the particulate beam attenuation spectrum and its inversion to
591 obtain the shape of the particulate size distribution, Appl. Opt., AO, 40(27), 4885–4893,
592 doi:10.1364/AO.40.004885, 2001.
593 Boyd, P. W. and Trull, T. W.: Understanding the export of biogenic particles in oceanic waters: Is there consensus?,
594 Progress in Oceanography, 72(4), 276–312, doi:10.1016/j.pocean.2006.10.007, 2007.
595 Boyd, P. W., Claustre, H., Levy, M., Siegel, D. A. and Weber, T.: Multi-faceted particle pumps drive carbon
596 sequestration in the ocean, Nature, 568(7752), 327–335, doi:10.1038/s41586-019-1098-2, 2019.
597 Buesseler, K. O. and Boyd, P. W.: Shedding light on processes that control particle export and flux attenuation in the
598 twilight zone of the open ocean, Limnology and Oceanography, 54(4), 1210–1232,
599 doi:10.4319/lo.2009.54.4.1210, 2009.
600 Cabré, A., Marinov, I. and Leung, S.: Consistent global responses of marine ecosystems to future climate change
601 across the IPCC AR5 earth system models, Clim Dyn, 45(5), 1253–1280, doi:10.1007/s00382-014-2374-3,
602 2015a.

https://doi.org/10.5194/bg-2020-156
Preprint. Discussion started: 25 May 2020

603 Cabré, A., Marinov, I., Bernardello, R. and Bianchi, D.: Oxygen minimum zones in the tropical Pacific across
604 CMIP5 models: mean state differences and climate change trends, Biogeosciences, 12(18), 5429–5454,
605 doi:10.5194/bg-12-5429-2015, 2015b.
606 Caesar, L., Rahmstorf, S., Robinson, A., Feulner, G. and Saba, V.: Observed fingerprint of a weakening Atlantic
607 Ocean overturning circulation, Nature, 556(7700), 191–196, doi:10.1038/s41586-018-0006-5, 2018.
608 Capotondi, A., Alexander, M. A., Bond, N. A., Curchitser, E. N. and Scott, J. D.: Enhanced upper ocean
609 stratification with climate change in the CMIP3 models, Journal of Geophysical Research: Oceans,
610 117(C4), doi:10.1029/2011JC007409, 2012.
611 Carr, M.-E., Friedrichs, M. A. M., Schmeltz, M., Noguchi Aita, M., Antoine, D., Arrigo, K. R., Asanuma, I.,
612 Aumont, O., Barber, R., Behrenfeld, M., Bidigare, R., Buitenhuis, E. T., Campbell, J., Ciotti, A., Dierssen,
613 H., Dowell, M., Dunne, J., Esaias, W., Gentili, B., Gregg, W., Groom, S., Hoepffner, N., Ishizaka, J.,
614 Kameda, T., Le Quéré, C., Lohrenz, S., Marra, J., Mélin, F., Moore, K., Morel, A., Reddy, T. E., Ryan, J.,
615 Scardi, M., Smyth, T., Turpie, K., Tilstone, G., Waters, K. and Yamanaka, Y.: A comparison of global
616 estimates of marine primary production from ocean color, Deep Sea Research Part II: Topical Studies in
617 Oceanography, 53(5), 741–770, doi:10.1016/j.dsr2.2006.01.028, 2006.
618 Cavan, E. L., Trimmer, M., Shelley, F. and Sanders, R.: Remineralization of particulate organic carbon in an ocean
619 oxygen minimum zone, Nature Communications, 8(1), 1–9, doi:10.1038/ncomms14847, 2017.
620 Cavan, E. L., Henson, S. A. and Boyd, P. W.: The Sensitivity of Subsurface Microbes to Ocean Warming
621 Accentuates Future Declines in Particulate Carbon Export, Front. Ecol. Evol., 6,
622 doi:10.3389/fevo.2018.00230, 2019.
623 Codispoti, L. A.: Interesting Times for Marine N2O, Science, 327(5971), 1339–1340, doi:10.1126/science.1184945,
624 2010.
625 Collins, M., An, S.-I., Cai, W., Ganachaud, A., Guilyardi, E., Jin, F.-F., Jochum, M., Lengaigne, M., Power, S.,
626 Timmermann, A., Vecchi, G. and Wittenberg, A.: The impact of global warming on the tropical Pacific
627 Ocean and El Niño, Nature Geoscience, 3(6), 391–397, doi:10.1038/ngeo868, 2010.
628 Collins, M., Sutherland, M., Bouwer, L., Cheong, S.-M., Frölicher, T., Jacot Des Combes, H., Koll Roxy, M.,
629 Losada, I., McInnes, K., Ratter, B., Rivera-Arriaga, E., Susanto, R. D., Swingedouw, D. and Tibig, L.:
630 Chapter 6: Extremes, Abrupt Changes and Managing Risks — Special Report on the Ocean and
631 Cryosphere in a Changing Climate. [online] Available from: https://www.ipcc.ch/srocc/chapter/chapter-6/
632 (Accessed 15 April 2020), 2019.
633 Cram, J. A., Weber, T., Leung, S. W., McDonnell, A. M. P., Liang, J.-H. and Deutsch, C.: The Role of Particle Size,
634 Ballast, Temperature, and Oxygen in the Sinking Flux to the Deep Sea, Global Biogeochemical Cycles,
635 32(5), 858–876, doi:10.1029/2017GB005710, 2018.
636 Devol, A. H. and Hartnett, H. E.: Role of the oxygen-deficient zone in transfer of organic carbon to the deep ocean,
637 Limnology and Oceanography, 46(7), 1684–1690, doi:10.4319/lo.2001.46.7.1684, 2001.

638 DeVries, T.: The oceanic anthropogenic CO2 sink: Storage, air-sea fluxes, and transports over the industrial era,
639 Global Biogeochemical Cycles, 28(7), 631–647, doi:10.1002/2013GB004739, 2014.
640 DeVries, T. and Primeau, F.: Dynamically and Observationally Constrained Estimates of Water-Mass Distributions
641 and Ages in the Global Ocean, J. Phys. Oceanogr., 41(12), 2381–2401, doi:10.1175/JPO-D-10-05011.1,
642 2011.
643 DeVries, T. and Weber, T.: The export and fate of organic matter in the ocean: New constraints from combining
644 satellite and oceanographic tracer observations, Global Biogeochemical Cycles, 31(3), 535–555,
645 doi:10.1002/2016GB005551, 2017.
646 DeVries, T., Liang, J.-H. and Deutsch, C.: A mechanistic particle flux model applied to the oceanic phosphorus
647 cycle, Biogeosciences, 11(19), 5381–5398, doi:https://doi.org/10.5194/bg-11-5381-2014, 2014.
648 Ducklow, H., Steinberg, D. and Buesseler, K.: Upper Ocean Carbon Export and the Biological Pump, oceanog,
649 14(4), 50–58, doi:10.5670/oceanog.2001.06, 2001.
650 Dugdale, R. and Wilkerson, F.: Nutrient Limitation of New Production in the Sea, in Primary Productivity and
651 Biogeochemical Cycles in the Sea, edited by P. G. Falkowski, A. D. Woodhead, and K. Vivirito, pp. 107–
652 122, Springer US, Boston, MA., 1992.
653 Dunne, J. P., Armstrong, R. A., Gnanadesikan, A. and Sarmiento, J. L.: Empirical and mechanistic models for the
654 particle export ratio, Global Biogeochemical Cycles, 19(4), doi:10.1029/2004GB002390, 2005.
655 Dunne, J. P., Sarmiento, J. L. and Gnanadesikan, A.: A synthesis of global particle export from the surface ocean
656 and cycling through the ocean interior and on the seafloor, Global Biogeochemical Cycles, 21(4),
657 doi:10.1029/2006GB002907, 2007.
658 Falkowski, P. G., Barber, R. T. and Smetacek, V.: Biogeochemical Controls and Feedbacks on Ocean Primary
659 Production, Science, 281(5374), 200–206, doi:10.1126/science.281.5374.200, 1998.
660 Friedland, K. D., Stock, C., Drinkwater, K. F., Link, J. S., Leaf, R. T., Shank, B. V., Rose, J. M., Pilskaln, C. H. and
661 Fogarty, M. J.: Pathways between Primary Production and Fisheries Yields of Large Marine Ecosystems,
662 PLoS One, 7(1), doi:10.1371/journal.pone.0028945, 2012.
663 Galbraith, E. D. and Martiny, A. C.: A simple nutrient-dependence mechanism for predicting the stoichiometry of
664 marine ecosystems, Proc. Natl. Acad. Sci. U.S.A., 112(27), 8199–8204, doi:10.1073/pnas.1423917112,
665 2015.
666 Gehlen, M., Bopp, L., Emprin, N., Aumont, O., Heinze, C. and Ragueneau, O.: Reconciling surface ocean
667 productivity, export fluxes and sediment composition in a global biogeochemical ocean model,
668 Biogeosciences, 3(4), 521–537, doi:https://doi.org/10.5194/bg-3-521-2006, 2006.
669 Gregg, W. W., Ginoux, P., Schopf, P. S. and Casey, N. W.: Phytoplankton and iron: validation of a global three-
670 dimensional ocean biogeochemical model, Deep Sea Research Part II: Topical Studies in Oceanography,
671 50(22), 3143–3169, doi:10.1016/j.dsr2.2003.07.013, 2003.

https://doi.org/10.5194/bg-2020-156
Preprint. Discussion started: 25 May 2020

672 Guidi, L., Stemmann, L., Legendre, L., Picheral, M., Prieur, L. and Gorsky, G.: Vertical distribution of aggregates
673 (>110 µm) and mesoscale activity in the northeastern Atlantic: Effects on the deep vertical export of
674 surface carbon, Limnology and Oceanography, 52(1), 7–18, doi:10.4319/lo.2007.52.1.0007, 2007.
675 Guidi, L., Jackson, G. A., Stemmann, L., Miquel, J. C., Picheral, M. and Gorsky, G.: Relationship between particle
676 size distribution and flux in the mesopelagic zone, Deep Sea Research Part I: Oceanographic Research
677 Papers, 55(10), 1364–1374, doi:10.1016/j.dsr.2008.05.014, 2008.
678 Guidi, L., Stemmann, L., Jackson, G. A., Ibanez, F., Claustre, H., Legendre, L., Picheral, M. and Gorskya, G.:
679 Effects of phytoplankton community on production, size, and export of large aggregates: A world-ocean
680 analysis, Limnology and Oceanography, 54(6), 1951–1963, doi:10.4319/lo.2009.54.6.1951, 2009.
681 Hartnett, H. E. and Devol, A. H.: Role of a strong oxygen-deficient zone in the preservation and degradation of
682 organic matter: a carbon budget for the continental margins of northwest Mexico and Washington State,
683 Geochimica et Cosmochimica Acta, 67(2), 247–264, doi:10.1016/S0016-7037(02)01076-1, 2003.
684 Henson, S. A., Sanders, R., Madsen, E., Morris, P. J., Moigne, F. L. and Quartly, G. D.: A reduced estimate of the
685 strength of the ocean's biological carbon pump, Geophysical Research Letters, 38(4),
686 doi:10.1029/2011GL046735, 2011.
687 Hirata, T., Hardman-Mountford, N. J., Brewin, R. J. W., Aiken, J., Barlow, R., Suzuki, K., Isada, T., Howell, E.,
688 Hashioka, T., Noguchi-Aita, M. and Yamanaka, Y.: Synoptic relationships between surface Chlorophyll-*a*
689 and diagnostic pigments specific to phytoplankton functional types, Biogeosciences, 8(2), 311–327,
690 doi:https://doi.org/10.5194/bg-8-311-2011, 2011.
691 Hofmann, M. and Schellnhuber, H.-J.: Oceanic acidification affects marine carbon pump and triggers extended
692 marine oxygen holes, PNAS, 106(9), 3017–3022, doi:10.1073/pnas.0813384106, 2009.
693 John, E. H., Wilson, J. D., Pearson, P. N. and Ridgwell, A.: Temperature-dependent remineralization and carbon
694 cycling in the warm Eocene oceans, Palaeogeography, Palaeoclimatology, Palaeoecology, 413, 158–166,
695 doi:10.1016/j.palaeo.2014.05.019, 2014.
696 Keeling, R. F., Körtzinger, A. and Gruber, N.: Ocean Deoxygenation in a Warming World, Annual Review of
697 Marine Science, 2(1), 199–229, doi:10.1146/annurev.marine.010908.163855, 2010.
698 Kostadinov, T. S., Siegel, D. A. and Maritorena, S.: Retrieval of the particle size distribution from satellite ocean
699 color observations, Journal of Geophysical Research: Oceans, 114(C9), doi:10.1029/2009JC005303, 2009.
700 Kriest, I. and Oschlies, A.: On the treatment of particulate organic matter sinking in large-scale models of marine
701 biogeochemical cycles, Biogeosciences, 5(1), 55–72, doi:https://doi.org/10.5194/bg-5-55-2008, 2008.
702 Kwon, E. Y., Primeau, F. and Sarmiento, J. L.: The impact of remineralization depth on the air–sea carbon balance,
703 Nature Geoscience, 2(9), 630–635, doi:10.1038/ngeo612, 2009.
704 Lam, P. J. and Bishop, J. K. B.: High biomass, low export regimes in the Southern Ocean, Deep Sea Research Part
705 II: Topical Studies in Oceanography, 54(5), 601–638, doi:10.1016/j.dsr2.2007.01.013, 2007.
706 Laufkötter, C., Vogt, M., Gruber, N., Aumont, O., Bopp, L., Doney, S. C., Dunne, J. P., Hauck, J., John, J. G., Lima,
707 I. D., Seferian, R. and Völker, C.: Projected decreases in future marine export production: the role of the

https://doi.org/10.5194/bg-2020-156
Preprint. Discussion started: 25 May 2020

carbon flux through the upper ocean ecosystem, Biogeosciences, 13(13), 4023–4047, doi:https://doi.org/10.5194/bg-13-4023-2016, 2016.

Laws, E. A., Falkowski, P. G., Smith, W. O., Ducklow, H. and McCarthy, J. J.: Temperature effects on export production in the open ocean, Global Biogeochemical Cycles, 14(4), 1231–1246, doi:10.1029/1999GB001229, 2000.

Laws, E. A., D'Sa, E. and Naik, P.: Simple equations to estimate ratios of new or export production to total production from satellite-derived estimates of sea surface temperature and primary production, Limnology and Oceanography: Methods, 9(12), 593–601, doi:10.4319/lom.2011.9.593, 2011.

Le Quéré, C., Harrison, S. P., Prentice, I. C., Buitenhuis, E. T., Aumont, O., Bopp, L., Claustre, H., Cunha, L. C. D., Geider, R., Giraud, X., Klaas, C., Kohfeld, K. E., Legendre, L., Manizza, M., Platt, T., Rivkin, R. B., Sathyendranath, S., Uitz, J., Watson, A. J. and Wolf-Gladrow, D.: Ecosystem dynamics based on plankton functional types for global ocean biogeochemistry models, Global Change Biology, 11(11), 2016–2040, doi:10.1111/j.1365-2486.2005.1004.x, 2005.

Lee, Z., Weidemann, A., Kindle, J., Arnone, R., Carder, K. L. and Davis, C.: Euphotic zone depth: Its derivation and implication to ocean-color remote sensing, Journal of Geophysical Research: Oceans, 112(C3), doi:10.1029/2006JC003802, 2007.

Letscher, R. T., Primeau, F. and Moore, J. K.: Nutrient budgets in the subtropical ocean gyres dominated by lateral transport, Nature Geoscience, 9(11), 815–819, doi:10.1038/ngeo2812, 2016.

Litchman, E., Klausmeier, C. A., Schofield, O. M. and Falkowski, P. G.: The role of functional traits and trade-offs in structuring phytoplankton communities: scaling from cellular to ecosystem level, Ecology Letters, 10(12), 1170–1181, doi:10.1111/j.1461-0248.2007.01117.x, 2007.

Locarnini, R. A., Mishonov, A. V., Antonov, J. I., Boyer, T. P., Garcia, H. E., Baranova, O. K., Zweng, M. M. and Johnson, D. R.: World Ocean Atlas 2009, Volume 1: Temperature, edited by S. Levitus, 2010.

Long, M. C., Deutsch, C. and Ito, T.: Finding forced trends in oceanic oxygen, Global Biogeochemical Cycles, 30(2), 381–397, doi:10.1002/2015GB005310, 2016.

Maier-Reimer, E.: Geochemical cycles in an ocean general circulation model. Preindustrial tracer distributions, Global Biogeochemical Cycles, 7(3), 645–677, doi:10.1029/93GB01355, 1993.

Marsay, C. M., Sanders, R. J., Henson, S. A., Pabortsava, K., Achterberg, E. P. and Lampitt, R. S.: Attenuation of sinking particulate organic carbon flux through the mesopelagic ocean, PNAS, 112(4), 1089–1094, doi:10.1073/pnas.1415311112, 2015.

Martin, J. H., Knauer, G. A., Karl, D. M. and Broenkow, W. W.: VERTEX: carbon cycling in the northeast Pacific, Deep Sea Research Part A. Oceanographic Research Papers, 34(2), 267–285, doi:10.1016/0198-0149(87)90086-0, 1987.

Martínez-García, A., Sigman, D. M., Ren, H., Anderson, R. F., Straub, M., Hodell, D. A., Jaccard, S. L., Eglinton, T. I. and Haug, G. H.: Iron Fertilization of the Subantarctic Ocean During the Last Ice Age, Science, 343(6177), 1347–1350, doi:10.1126/science.1246848, 2014.

https://doi.org/10.5194/bg-2020-156
Preprint. Discussion started: 25 May 2020


Biogeosciences Discussions Open Access EGU

744 Matear, R. J. and Hirst, A. C.: Long-term changes in dissolved oxygen concentrations in the ocean caused by
745 protracted global warming, Global Biogeochemical Cycles, 17(4), doi:10.1029/2002GB001997, 2003.
746 Matsumoto, K.: Biology-mediated temperature control on atmospheric pCO2 and ocean biogeochemistry,
747 Geophysical Research Letters, 34(20), doi:10.1029/2007GL031301, 2007a.
748 Matsumoto, K.: Radiocarbon-based circulation age of the world oceans, Journal of Geophysical Research: Oceans,
749 112(C9), doi:10.1029/2007JC004095, 2007b.
750 McDonnell, A. M. P. and Buesseler, K. O.: Variability in the average sinking velocity of marine particles,
751 Limnology and Oceanography, 55(5), 2085–2096, doi:10.4319/lo.2010.55.5.2085, 2010.
752 McDonnell, A. M. P., Boyd, P. W. and Buesseler, K. O.: Effects of sinking velocities and microbial respiration rates
753 on the attenuation of particulate carbon fluxes through the mesopelagic zone, Global Biogeochemical
754 Cycles, 29(2), 175–193, doi:10.1002/2014GB004935, 2015.
755 Michaels, A. F. and Silver, M. W.: Primary production, sinking fluxes and the microbial food web, Deep Sea
756 Research Part A. Oceanographic Research Papers, 35(4), 473–490, doi:10.1016/0198-0149(88)90126-4,
757 1988.
758 Moore, J. K., Fu, W., Primeau, F., Britten, G. L., Lindsay, K., Long, M., Doney, S. C., Mahowald, N., Hoffman, F.
759 and Randerson, J. T.: Sustained climate warming drives declining marine biological productivity, Science,
760 359(6380), 1139–1143, doi:10.1126/science.aao6379, 2018.
761 Najjar, R. G., Sarmiento, J. L. and Toggweiler, J. R.: Downward transport and fate of organic matter in the ocean:
762 Simulations with a general circulation model, Global Biogeochemical Cycles, 6(1), 45–76,
763 doi:10.1029/91GB02718, 1992.
764 Oschlies, A., Schulz, K. G., Riebesell, U. and Schmittner, A.: Simulated 21st century's increase in oceanic suboxia
765 by CO2-enhanced biotic carbon export, Global Biogeochemical Cycles, 22(4),
766 doi:10.1029/2007GB003147, 2008.
767 Passow, U. and Carlson, C. A.: The biological pump in a high CO2 world, Marine Ecology Progress Series, 470,
768 249–271, doi:10.3354/meps09985, 2012.
769 Picheral, M., Guidi, L., Stemmann, L., Karl, D. M., Iddaoud, G. and Gorsky, G.: The Underwater Vision Profiler 5:
770 An advanced instrument for high spatial resolution studies of particle size spectra and zooplankton,
771 Limnology and Oceanography: Methods, 8(9), 462–473, doi:10.4319/lom.2010.8.462, 2010.
772 Rossow, W. B. and Schiffer, R. A.: Advances in Understanding Clouds from ISCCP, Bull. Amer. Meteor. Soc.,
773 80(11), 2261–2288, doi:10.1175/1520-0477(1999)080<2261:AIUCFI>2.0.CO;2, 1999.
774 Sarmiento, J. L. and Siegenthaler, U.: New Production and the Global Carbon Cycle, in Primary Productivity and
775 Biogeochemical Cycles in the Sea, edited by P. G. Falkowski, A. D. Woodhead, and K. Vivirito, pp. 317–
776 332, Springer US, Boston, MA., 1992.
777 Schmidtko, S., Stramma, L. and Visbeck, M.: Decline in global oceanic oxygen content during the past five decades,
778 Nature, 542(7641), 335–339, doi:10.1038/nature21399, 2017.

https://doi.org/10.5194/bg-2020-156
Preprint. Discussion started: 25 May 2020

779 Schmittner, A., Oschlies, A., Giraud, X., Eby, M. and Simmons, H. L.: A global model of the marine ecosystem for
780 long-term simulations: Sensitivity to ocean mixing, buoyancy forcing, particle sinking, and dissolved
781 organic matter cycling, Global Biogeochemical Cycles, 19(3), doi:10.1029/2004GB002283, 2005.
782 Sheldon, R. W., Prakash, A. and Sutcliffe, W. H.: The Size Distribution of Particles in the Ocean1, Limnology and
783 Oceanography, 17(3), 327–340, doi:10.4319/lo.1972.17.3.0327, 1972.
784 Siegel, D. A., Buesseler, K. O., Doney, S. C., Sailley, S. F., Behrenfeld, M. J. and Boyd, P. W.: Global assessment
785 of ocean carbon export by combining satellite observations and food-web models, Global Biogeochemical
786 Cycles, 28(3), 181–196, doi:10.1002/2013GB004743, 2014.
787 Smayda, T. J.: Normal and accelerated sinking of phytoplankton in the sea, Marine Geology, 11(2), 105–122,
788 doi:10.1016/0025-3227(71)90070-3, 1971.
789 Smith, T. M., Reynolds, R. W., Peterson, T. C. and Lawrimore, J.: Improvements to NOAA's Historical Merged
790 Land–Ocean Surface Temperature Analysis (1880–2006), J. Climate, 21(10), 2283–2296,
791 doi:10.1175/2007JCLI2100.1, 2008.
792 Steinberg, D. K., Lomas, M. W. and Cope, J. S.: Long-term increase in mesozooplankton biomass in the Sargasso
793 Sea: Linkage to climate and implications for food web dynamics and biogeochemical cycling, Global
794 Biogeochemical Cycles, 26(1), doi:10.1029/2010GB004026, 2012.
795 Thornton, D. C. O.: Dissolved organic matter (DOM) release by phytoplankton in the contemporary and future
796 ocean, European Journal of Phycology, 49(1), 20–46, doi:10.1080/09670262.2013.875596, 2014.
797 Toggweiler, J. R. and Russell, J.: Ocean circulation in a warming climate, Nature, 451(7176), 286–288,
798 doi:10.1038/nature06590, 2008.
799 Turner, J. T.: Zooplankton fecal pellets, marine snow, phytodetritus and the ocean's biological pump, Progress in
800 Oceanography, 130, 205–248, doi:10.1016/j.pocean.2014.08.005, 2015.
801 Van Mooy, B. A. S., Keil, R. G. and Devol, A. H.: Impact of suboxia on sinking particulate organic carbon:
802 Enhanced carbon flux and preferential degradation of amino acids via denitrification, Geochimica et
803 Cosmochimica Acta, 66(3), 457–465, doi:10.1016/S0016-7037(01)00787-6, 2002.
804 Weber, T. and Deutsch, C.: Oceanic nitrogen reservoir regulated by plankton diversity and ocean circulation,
805 Nature, 489(7416), 419–422, doi:10.1038/nature11357, 2012.
806 Weber, T. and Deutsch, C.: Local versus basin-scale limitation of marine nitrogen fixation, Proceedings of the
807 National Academy of Sciences, 111(24), 8741–8746, doi:10.1073/pnas.1317193111, 2014.
808 Weber, T., Cram, J. A., Leung, S. W., DeVries, T. and Deutsch, C.: Deep ocean nutrients imply large latitudinal
809 variation in particle transfer efficiency, PNAS, 113(31), 8606–8611, doi:10.1073/pnas.1604414113, 2016.
810 Yamanaka, Y. and Tajika, E.: The role of the vertical fluxes of particulate organic matter and calcite in the oceanic
811 carbon cycle: Studies using an ocean biogeochemical general circulation model, Global Biogeochemical
812 Cycles, 10(2), 361–382, doi:10.1029/96GB00634, 1996.
813

https://doi.org/10.5194/bg-2020-156
Preprint. Discussion started: 25 May 2020

Biogeosciences
Discussions
Open Access
EGU

814

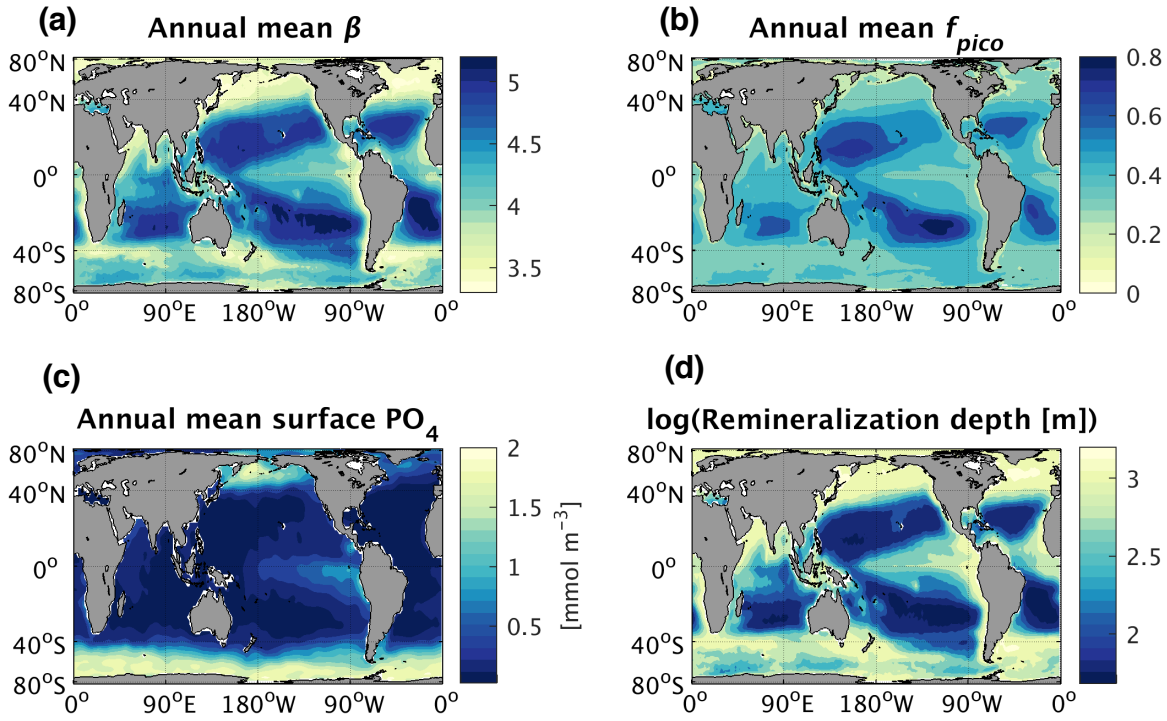

815

816 **Figure 1: Global maps of annual mean (a) particle size distribution slope (β) measured by remotely-sensed particulate**
817 **backscatter and reproduced from Kostadinov et al. (2009), (b) fractional picophytoplankton abundance (fpico) reproduced**
818 **from Hirata et al. (2011), (c) surface phosphate concentration from World Ocean Atlas, and (d) remineralization depth,**
819 **defined as the depth at which particulate flux out of the euphotic zone is decreased by a factor of e assuming β in (a) at the**
820 **surface, calculated using a particle remineralization and sinking model (PRiSM, described in Section 2.1.1).**

821

https://doi.org/10.5194/bg-2020-156
Preprint. Discussion started: 25 May 2020

Biogeosciences
Discussions
Open Access
EGU

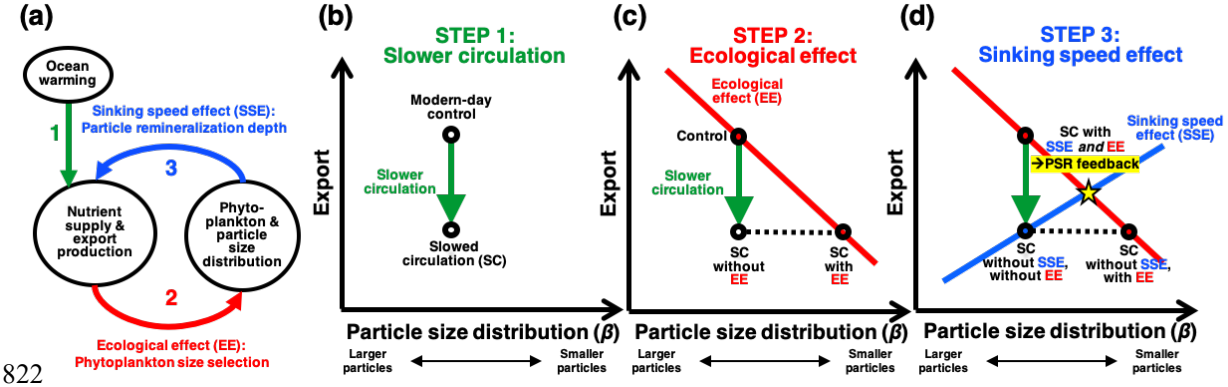

Figure 2: (a) Schematic diagram of the particle size-remineralization (PSR) negative feedback on export production. A change in circulation rates induced by climate change alters surface nutrient supply and subsequent export production (green arrow). Changes in surface nutrient supply also drive changes in phytoplankton and resultant sinking particle sizes (red arrow). Changes in sinking particle sizes in turn alter remineralization depth and consequently, surface nutrient supply and export (blue arrow). (b) Schematic depicting decreased export production with decreases in circulation rates and surface nutrient supply. (c) Schematic depicting a theoretical relationship between export and β, here termed the phytoplankton size selection ecological effect (EE), in which smaller phytoplankton dominate in low-nutrient, low-export conditions. (d) Schematic depicting all previous components of the PSR feedback, in addition to the crucial final component: the particle remineralization depth sinking speed effect (SSE), in which smaller particles tend to get remineralized shallower, leading to a greater recycled surface nutrient supply and therefore greater export.

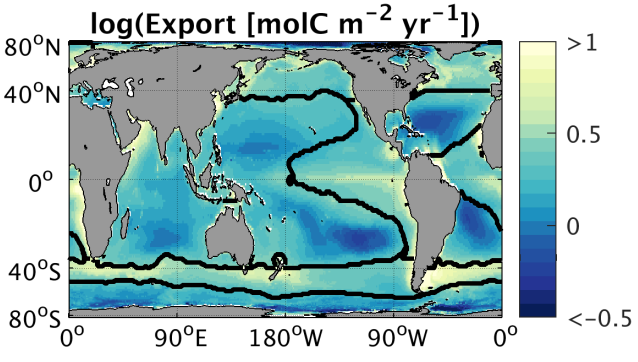

Figure 3: Global map of regionally-weighted annual mean export, averaged over nine different export maps (detailed in Section 2.2.2). Contours indicate biogeochemical regions used for weighting and spatial averaging.

https://doi.org/10.5194/bg-2020-156
Preprint. Discussion started: 25 May 2020

Biogeosciences
Discussions
Open Access
EGU

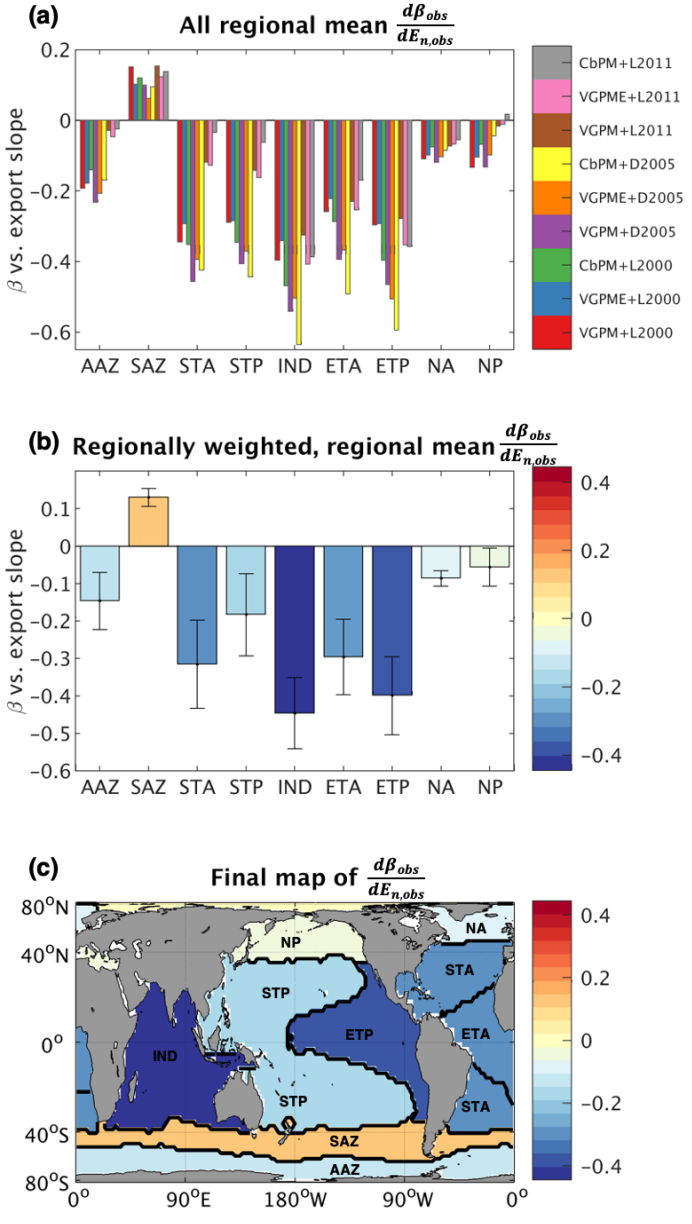

838

839 **Figure 4: (a) Regional mean changes in particle size slope for a given change in time-mean normalized export, $\frac{d\beta_{obs}}{dE_{n,obs}}$ (i.e.,**
840 **spatial averages of each map in Fig. S3 over regions shown in Fig. 3), colored by corresponding export map. Colorbar labels**
841 **indicate the NPP and e-ratio algorithms used to generate the given export map (see Section 2.2.2 for full descriptions of the**
842 **algorithms). (b) Regionally-weighted mean $\frac{d\beta_{obs}}{dE_{n,obs}}$, averaged over the nine possibilities for each region shown in (a). Error**
843 **bars represent one weighted standard deviation. (c) Global map of regionally variable $\frac{d\beta_{obs}}{dE_{n,obs}}$ used in model runs with the**
844 **PSR feedback on.**

https://doi.org/10.5194/bg-2020-156
Preprint. Discussion started: 25 May 2020

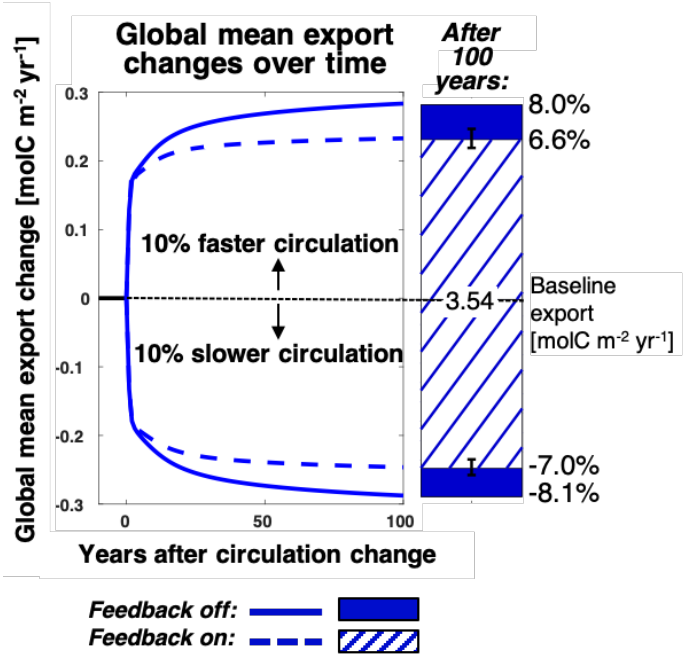

Figure 5: Changes in global mean export over time from baseline conditions (current-day circulation, ran to steady-state) after increasing or decreasing circulation rates by 10%. Dashed and solid lines represent runs with the PSR feedback turned off and on, respectively. The bars on the right show absolute changes in global mean export from the baseline case 100 years after changing circulation rates. Corresponding relative changes (calculated as absolute changes from the baseline over the baseline mean) are listed in black. Global mean export in the baseline case is listed on the zero line. Hatched and solid patterns represent runs with the PSR feedback turned off and on, respectively. The error bars represent export decreases generated when employing the upper and lower-bound $\frac{d\beta_{obs}}{dE_{n,obs}}$ maps described in Section 2.2.3.

https://doi.org/10.5194/bg-2020-156
Preprint. Discussion started: 25 May 2020

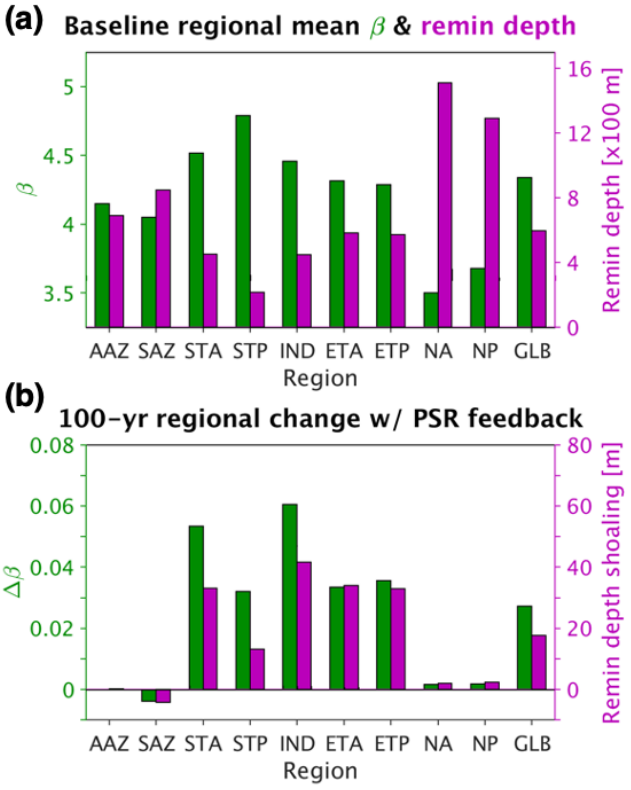

Figure 6: (a) Baseline (current-day circulation, ran to steady-state) regional mean β (shown in green) and e-folding remineralization depth (shown in purple). (b) Absolute change in regional mean β (shown in green) and absolute shoaling of regional mean remineralization depth (shown in purple) 100 years after decreasing circulation rates by 10% with the PSR feedback turned on.

https://doi.org/10.5194/bg-2020-156
Preprint. Discussion started: 25 May 2020

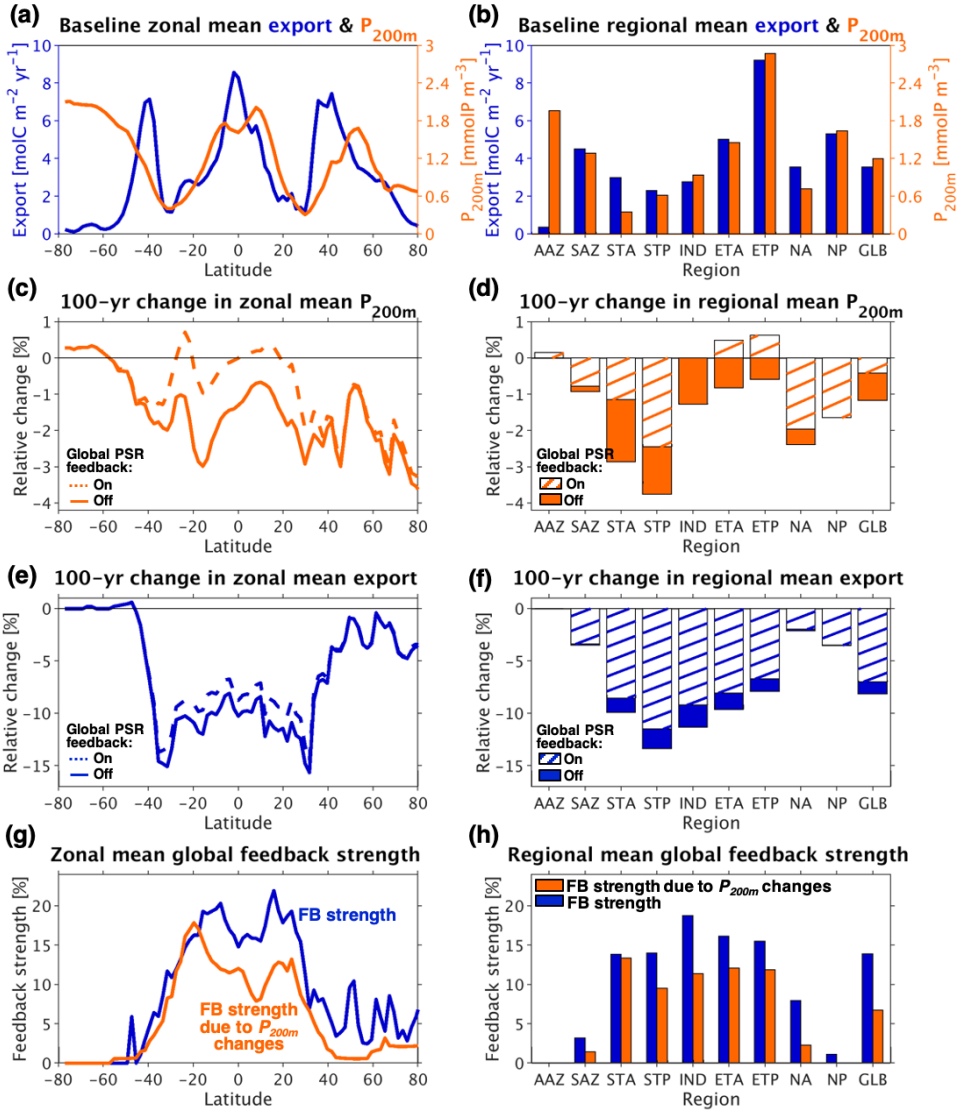

Figure 7: (a) Baseline (current-day circulation, ran to steady-state) zonal mean export and shallow subsurface (200 m) phosphate concentration. (b) Same as (a), but with regional and global rather than zonal means. (c) Relative changes (calculated as absolute changes from the baseline over the baseline mean) in zonal mean phosphate concentration at 200 m depth 100 years after decreasing circulation rates by 10%. (d) Same as (c), but with regional and global means. (e) Relative changes in zonal mean export 100 years after decreasing circulation rates by 10%. (f) Same as (e), but with regional and global means. (g) Zonal mean PSR feedback strength, calculated as the difference in zonal mean export change from baseline between the feedback-off and on cases divided by the zonal mean export change in the feedback-off case alone (left-hand side of Eq. (4); shown in blue). Predicted zonal mean PSR feedback strength from changes in circulation and shallow subsurface phosphate concentration (right-hand side of Eq. (4); shown in orange). (h) Same as (g), but with regional and global means.

https://doi.org/10.5194/bg-2020-156
Preprint. Discussion started: 25 May 2020

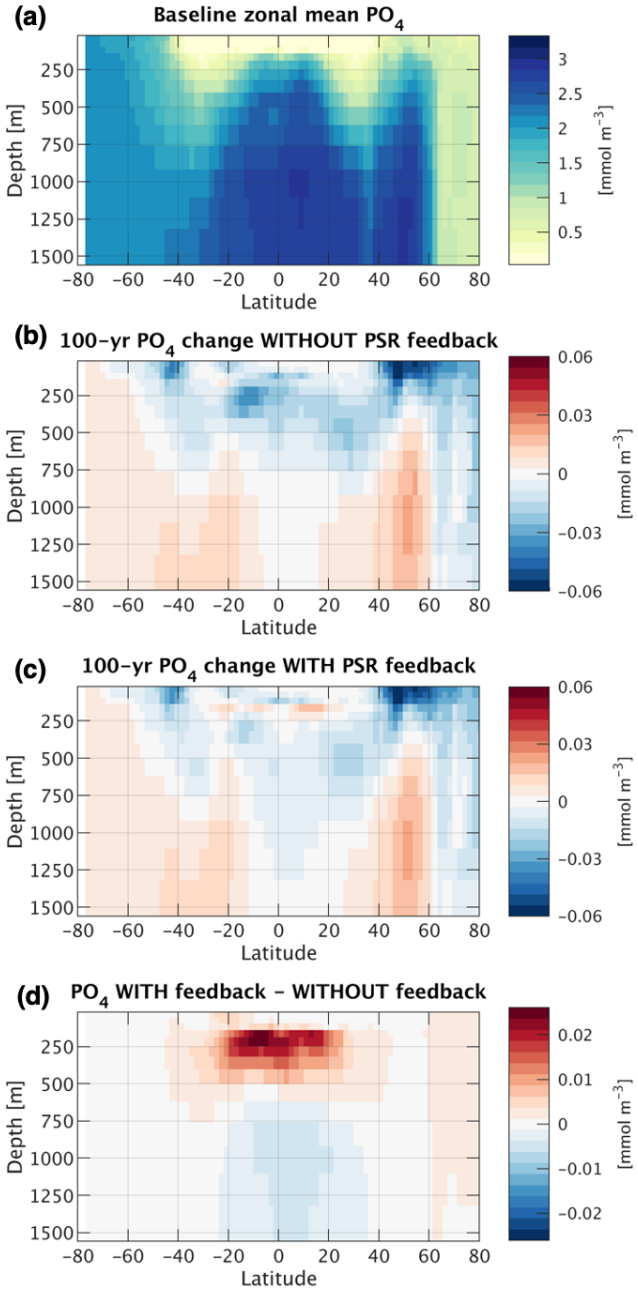

872

873 **Figure 8: (a) Baseline (current-day circulation, ran to steady-state) zonal mean phosphate concentration. (b) Absolute**
874 **change in zonal mean phosphate concentration 100 years after decreasing circulation rates by 10% with the PSR feedback**
875 **turned off. (c) Same as (b), but with the PSR feedback turned on. (d) Difference in zonal mean phosphate concentration**
876 **between PSR feedback-on and -off runs (i.e., (b) minus (c)).**

https://doi.org/10.5194/bg-2020-156
Preprint. Discussion started: 25 May 2020

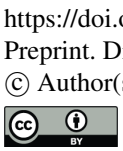

Biogeosciences
Discussions
Open Access
EGU

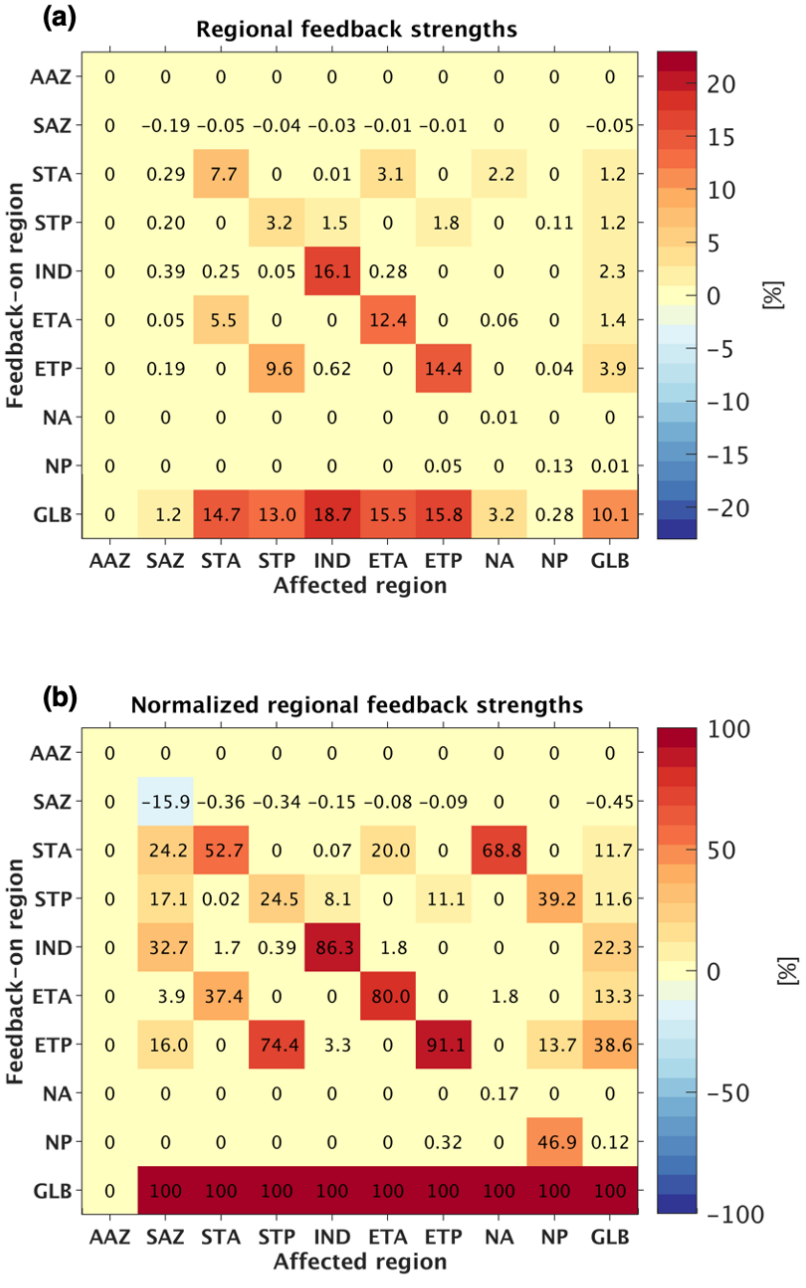

877

878 **Figure 9: (a) Regional mean PSR feedback strength due to the PSR feedback effect within each individual region. The y-**
879 **axis denotes the single region (or the entire ocean in the case of "GLB" or "global") within which the PSR feedback was**
880 **turned on, while the x-axis denotes the region affected. (b) Percent contribution of each individual region to each region's**
881 **total PSR feedback strength, computed as the regionally-derived feedback strength within an affected region divided by**
882 **the globally-derived feedback strength in the same affected region (i.e., each given grid cell in (a) is divided by the**
883 **corresponding column's bottom-most grid cell).**